Earth Syst. Sci. Data, 17, 2887–2909, 2025
https://doi.org/10.5194/essd-17-2887-2025

Open Access Earth System Science Data

Permafrost–wildfire interactions: active layer thickness estimates for paired burned and unburned sites in northern high latitudes

Anna C. Talucci[1], Michael M. Loranty[2], Jean E. Holloway[3], Brendan M. Rogers[1], Heather D. Alexander[4], Natalie Baillargeon[1], Jennifer L. Baltzer[5], Logan T. Berner[6], Amy Breen[7], Leya Brodt[8], Brian Buma[9,10], Jacqueline Dean[1], Clement J. F. Delcourt[11], Lucas R. Diaz[11], Catherine M. Dieleman[12], Thomas A. Douglas[13], Gerald V. Frost[14], Benjamin V. Gaglioti[15], Rebecca E. Hewitt[16], Teresa Hollingsworth[17,18], M. Torre Jorgenson[19], Mark J. Lara[20], Rachel A. Loehman[21], Michelle C. Mack[22], Kristen L. Manies[23], Christina Minions[1], Susan M. Natali[1], Jonathan A. O'Donnell[24], David Olefeldt[25], Alison K. Paulson[26], Adrian V. Rocha[27], Lisa B. Saperstein[28], Tatiana A. Shestakova[29,30,1], Seeta Sistla[31], Oleg Sizov[32], Andrey Soromotin[8], Merritt R. Turetsky[33], Sander Veraverbeke[11], and Michelle A. Walvoord[34]

[1]Woodwell Climate Research Center, Falmouth, MA 02540-1644, USA
[2]Department of Geography, Colgate University, Hamilton, NY 13346, USA
[3]Department of Geography, Environment and Geomatics, University of Ottawa, Ottawa, K1N 6N5, Canada
[4]College of Forestry, Wildlife, and Environment, Auburn University, Auburn, AL 36949, USA
[5]Biology Department, Wilfrid Laurier University, Waterloo, ON, N2L 3C5, Canada
[6]School of Informatics, Computing, and Cyber Systems, Northern Arizona University, Flagstaff, AZ 86011, USA
[7]International Arctic Research Center, University of Alaska Fairbanks, Fairbanks, AK 99775-7340, USA
[8]Research Institute of Ecology and Natural Resources Management, Tyumen State University, Tyumen, 625003, Russia
[9]Integrative Biology, University of Colorado (Denver), Boulder, CO 80304, USA
[10]Environmental Defense Fund, Boulder, CO 80302, USA
[11]Faculty of Science, Vrije Universiteit Amsterdam, Amsterdam, 1081 HV, the Netherlands
[12]School of Environmental Sciences, University of Guelph, Guelph, ON, N3H3Y8, Canada
[13]US Army Cold Regions Research and Engineering Laboratory, Fort Wainwright, AK 99703, USA
[14]Alaska Biological Research, Inc., Fairbanks, AK 99708, USA
[15]Water and Environmental Research Center, University of Alaska Fairbanks, Fairbanks, AK 99775, USA
[16]Department of Environmental Studies, Amherst College, Amherst, MA 01002, USA
[17]Pacific Northwest Research Station, USDA Forest Service, University of Alaska Fairbanks, Fairbanks, AK 99708, USA
[18]Aldo Leopold Wilderness Research Institute, Rocky Mountain Research Station, Missoula, MT 59801, USA
[19]Alaska Ecoscience, Fairbanks, AK 99775, USA
[20]Department(s) of Plant Biology and Geography, University of Illinois Urbana-Champaign, Urbana, IL 61801, USA
[21]US Geological Survey, Alaska Science Center, Anchorage, AK 99508, USA
[22]Center for Ecosystem Science and Society and Department of Biological Sciences, Northern Arizona University, Flagstaff, AZ 86001, USA
[23]US Geological Survey, Moffett Field, CA 94035, USA
[24]Arctic Network, National Park Service, Anchorage, AK 99501, USA
[25]Department of Renewable Resources, University of Alberta, Edmonton, AB, T6G 2G7, Canada
[26]Humboldt-Toiyabe National Forest, US Forest Service, Sparks, NV 89431, USA
[27]Department of Biological Sciences, University of Notre Dame, Notre Dame, IN 46556, USA

Published by Copernicus Publications.

[28]Alaska Regional Office, US Fish and Wildlife Service, Anchorage, AK 99503, USA
[29]Department of Agricultural and Forest Sciences and Engineering, University of Lleida, Av. Alcalde Rovira Roure 191, Lleida, Catalonia, 25198, Spain
[30]Joint Research Unit CTFC–AGROTECNIO–CERCA, Av. Alcalde Rovira Roure 191, Lleida, Catalonia, 25198, Spain
[31]Natural Resources Management & Environmental Sciences, Cal Poly, San Luis Obispo, CA 93401, USA
[32]Oil and Gas Research Institute RAS, Moscow, 119333, Russia
[33]Renewable and Sustainable Energy Institute, Department of Ecology and Evolutionary Biology, University of Colorado Boulder, Boulder, CO 80309-0552, USA
[34]US Geological Survey, Earth System Processes Division, Denver, CO 80225, USA

Correspondence: Anna C. Talucci (atalucci@woodwellclimate.org)

Received: 8 November 2024 – Discussion started: 3 December 2024
Revised: 24 February 2025 – Accepted: 19 March 2025 – Published: 26 June 2025

Abstract. As the northern high-latitude permafrost zone experiences accelerated warming, permafrost has become vulnerable to widespread thaw. Simultaneously, wildfire activity across northern boreal forest and Arctic/subarctic tundra regions impacts permafrost stability through the combustion of insulating organic matter, vegetation, and post-fire changes in albedo. Efforts to synthesis the impacts of wildfire on permafrost are limited and are typically reliant on antecedent pre-fire conditions. To address this, we created the FireALT dataset by soliciting data contributions that included thaw depth measurements, site conditions, and fire event details with paired measurements at environmentally comparable burned and unburned sites. The solicitation resulted in 52 466 thaw depth measurements from 18 contributors across North America and Russia. Because thaw depths were taken at various times throughout the thawing season, we also estimated end-of-season active layer thickness (ALT) for each measurement using a modified version of the Stefan equation. Here, we describe our methods for collecting and quality-checking the data, estimating ALT, the data structure, strengths and limitations, and future research opportunities. The final dataset includes 48 669 ALT estimates with 32 attributes across 9446 plots and 157 burned–unburned pairs spanning Canada, Russia, and the United States. The data span fire events from 1900 to 2022 with measurements collected from 2001 to 2023. The time since fire ranges from 0 to 114 years. The FireALT dataset addresses a key challenge: the ability to assess impacts of wildfire on ALT when measurements are taken at various times throughout the thaw season depending on the time of field campaigns (typically June through August) by estimating ALT at the end-of-season maximum. This dataset can be used to address understudied research areas, particularly algorithm development, calibration, and validation for evolving process-based models as well as extrapolating across space and time, which could elucidate permafrost–wildfire interactions under accelerated warming across the high-northern-latitude permafrost zone. The FireALT dataset is available through the Arctic Data Center (https://doi.org/10.18739/A2RN3092P, Talucci et al., 2024).

1 Introduction

Permafrost, defined as ground that remains at or below 0 °C for 2 or more consecutive years, has become vulnerable to widespread thaw in response to rapid climate warming at high latitudes. Permafrost temperatures have increased over the last 30 years (Romanovsky et al., 2010; Smith et al., 2010; Calvin et al., 2023), resulting in the thickening of the active layer, which is the uppermost, seasonally thawed layer (Harris et al., 1988; Bonnaventure and Lamoureux, 2013). Widespread permafrost thaw and increases in active layer thickness are expected under future climate conditions (Smith and Burgess, 2004; Zhang et al., 2008; Derksen et al., 2019; Peng et al., 2023), and these processes are expected to release large amounts of soil carbon to the atmosphere as greenhouse gas emissions (Schaefer et al., 2014; Gasser et al., 2018; Knoblauch et al., 2018; Yokohata et al., 2020; Natali et al., 2021; Schuur et al., 2022; See et al., 2024). Changes to permafrost, particularly near-surface permafrost and the active layer, have important implications for ecology, forestry, hydrology, biogeochemistry, climate feedbacks, engineering, traditional livelihoods, and community safety (Anisimov and Reneva, 2006; O'Donnell et al., 2011b; Rocha and Shaver, 2011; Bret-Harte et al., 2013; Hugelius et al., 2014; Jones et al., 2015; Li et al., 2019; Turetsky et al., 2020; Gibson et al., 2021; Huang et al., 2024).

Climate change is also intensifying high-latitude wildfire regimes (Kasischke et al., 2010; de Groot et al., 2013; Zhang et al., 2015; Wotton et al., 2017; Hanes et al., 2019; McCarty et al., 2021; Descals et al., 2022; Phillips et al.,

2022; Scholten et al., 2022; Zheng et al., 2023; Byrne et al., 2024). Wildfire activity shows interannual variability that is predominantly controlled by subseasonal drying and climate, where prolonged warm and dry conditions in conjunction with fuel accumulation may alter fire regimes and the seasonality of fire (York et al., 2020). The interaction between wildfire and permafrost results in both immediate and long-term effects on the surface energy balance and ground thermal regimes, as well as hydrologic cycling and soil and aquatic biogeochemistry (O'Donnell et al., 2011b; Rocha and Shaver, 2011; Bret-Harte et al., 2013; Jones et al., 2015; Li et al., 2019; Hollingsworth et al., 2020; Holloway et al., 2020). These interactions also result in second-order greenhouse gas emissions (O'Donnell et al., 2011c; Jiang et al., 2015; Smith et al., 2015; Jones et al., 2015; Gibson et al., 2018; Li et al., 2019) by making stored soil carbon available for mineralization (O'Donnell et al., 2011c; Rocha and Shaver, 2011; Bret-Harte et al., 2013; Hugelius et al., 2014; Jones et al., 2015; Li et al., 2019). Biomass combustion during fires removes the insulating surface vegetation (i.e., moss, lichen, low-growing shrubs) and soil organic matter, typically reduces evapotranspiration (Rouse, 1976; Amiro, 2001; Chambers and Chapin, 2002; Chambers et al., 2005; Amiro et al., 2006; Chebykina et al., 2022; Fedorov, 2022), and reduces short-term albedo during the thaw season, resulting in increases in the ground heat flux and the expansion of the active layer (Moskalenko, 1999; Rocha et al., 2012; Jafarov et al., 2013; Nossov et al., 2013; Jiang et al., 2015; Douglas et al., 2016; Fisher et al., 2016; Gibson et al., 2018). Similarly, tree canopy removal reduces shading in the summer and results in more snow on the ground in the winter, both leading to higher surface soil temperatures and expansion of the active layer into near-surface permafrost, which has been shown across North America (Rocha et al., 2012; Jafarov et al., 2013; Jiang et al., 2015; Zhang et al., 2015; Douglas et al., 2016; Fisher et al., 2016; Gibson et al., 2018) and Eurasia (Moskalenko, 1999; Lytkina, 2008; Kirdyanov et al., 2020; Heim et al., 2021; Fedorov, 2022; Petrov et al., 2022). In contrast, across North American Arctic tundra, shrub removal from wildfire results in thinner snow due to increased wind exposure, which causes a reduction of the active layer (Wang et al., 2012; Jones et al., 2024), while Russian scientists note an expansion of the seasonal active layer that is dependent on vegetation communities (Moskalenko, 1999; Lytkina, 2008).

Post-fire changes in the energy balance and subsequent increases in the active layer thickness have historically recovered to pre-fire conditions as vegetation succession occurred (Rouse, 1976; Amiro, 2001; Liu et al., 2005; Amiro et al., 2006), with a maximum active layer thickness often observed 5–10 years post-fire (Rocha et al., 2012; Holloway et al., 2020), but this may extend up to 30 or more years post-fire (Gibson et al., 2018; Kirdyanov et al., 2020; Heim et al., 2021). However, this pattern of recovery may be changing alongside climate warming and shifting fire regimes (Brown et al., 2015), and it may be further impacted by secondary disturbances (Hayes and Buma, 2021). For example, as wildfire burns across permafrost peatlands, there is not only a thicker and warmer active layer but also an expansion of year-round unfrozen ground (i.e., taliks) and thermokarst bogs (Gibson et al., 2018). These changes in active layer thickness and hydrologic dynamics can constrain regeneration by prolonging vegetation recovery and inducing shifts in vegetation composition and structure (Baltzer et al., 2014; Dearborn et al., 2021). Further, near-surface permafrost degradation can lead to ground subsidence, which alters surface hydrology, often leading to water inundation and further degradation (Brown et al., 2015). Where wildfires burn across permafrost landforms (e.g., thermokarst, ice-rich areas), deep and irreversible thawing could permanently alter the landscape (Burn and Lewkowicz, 1990; Lewkowicz, 2007; Sannel and Kuhry, 2011; Liljedahl et al., 2016; Rudy et al., 2017; Borge et al., 2017; Mamet et al., 2017; Fraser et al., 2018), releasing long-stored soil carbon into the atmosphere (Schuur et al., 2015). Currently, emissions from fire-induced permafrost thaw are underestimated by the scientific community and climate models (Natali et al., 2021; Treharne et al., 2022; Schädel et al., 2024), an issue that is exacerbated by modeling challenges and uncertainties associated with permafrost carbon stocks (Hugelius et al., 2014; Turetsky et al., 2020). The change in active layer thickness over time is a critical diagnostic indicator of permafrost conditions (Brown et al., 2000; Shiklomanov et al., 2010) and a vital component of modeling carbon emissions from fire- and non-fire-related permafrost thaw.

To provide critical data that can be used for understanding and modeling impacts of wildfire on permafrost, we compiled a dataset of thaw depth measurements from paired burned and unburned sites across the northern high-latitude permafrost zone. This dataset is the first of its kind to focus on paired burned and unburned sites providing a circumpolar/boreal perspective. Climate and ecosystem conditions including drainage, vegetation, and soil characteristics control near-surface permafrost characteristics, and thus in order to detect an influence of wildfire it is necessary to have measurements either pre- and post-fire or unburned control and nearby burned sites with otherwise similar ecosystem properties. Measuring ALT for paired unburned control and nearby burn sites is more realistic due to the stochasticity of wildfire. Further, unburned control sites provide a benchmark for understanding the impact of wildfire in these dynamic systems. Thaw depth increases over the course of the thawing season until it reaches its maximum depth, i.e., active layer thickness (ALT). This means that early-season to mid-season measurements do not capture the full depth of the thawed active layer. As such, the variability in thawing season and measurement timing makes it difficult to compare across space and time. Therefore, we standardized thaw depths taken at different times throughout the thawing season, which resulted in an estimated dataset of ALT. Further, capturing the maximum ALT aids in establishing the full scope of permafrost

change because it is a critical indicator of thaw dynamics. Depending on the location ALT could occur anywhere from August through November. The overarching goal is to generate a synthesized dataset of ALT for burned–unburned pairs. To achieve this, we had four main objectives for the paper: (1) describe how the data were collected and synthesized for thaw depth measurements of burned sites with paired unburned sites; (2) describe how we standardized thaw depth measurements to end-of-season ALT with estimates of uncertainty; (3) provide details on how to aggregate data to plot, site, and paired burned–unburned means and provide a summary of the dataset; and (4) discuss the strengths and limitations of the dataset, along with its potential uses.

2 Data and methods

2.1 Data solicitation and quality screening

To assemble a dataset capable of widely characterizing the influence of wildfire on permafrost, we solicited field measurements of thaw depth from paired burned and unburned sites from researchers working in boreal forest and tundra ecosystems. Thaw depth refers to the depth or thickness of the unfrozen surface soil layer anytime during the thawing season. The datasets that contribute to this synthesis were obtained by measuring depth to refusal using a graduated steel probe (Brown et al., 2000). A steel probe is a typical means of measurements; however, there is potential for error introduced by issues such as identifying the freeze–thaw boundary, soil variability, subsidence, and user bias (Brown et al., 200; Bonnaventure and Lamoureux, 2013; Strand et al., 2021; Scheer et al., 2023). A critical component of the data required an ecologically appropriate unburned site(s) within close proximity that shared similar dominant vegetation, drainage, and climatic conditions to be paired with one or more burned sites, meaning the burned site would have had similar pre-fire conditions to the unburned site. We began by soliciting data from members of the Permafrost Carbon Network and their collaborators and then used a literature review to identify additional contributors. Data contributors were required to submit metadata (Table S1 in the Supplement) and data via a Google form with required attributes that included their last name, country where data were collected, latitude, longitude, biome, vegetation cover class, site identifier, plot identifier, year data were collected, month data were collected, day data were collected, fire identifier, fire year, whether the site was burned or unburned, organic layer depth, thaw depth, whether the probe hit rock, whether the depth was greater than the probe, contributors assigned a designation of "thaw" or "active" to indicate early–middle- or late-season measurements, respectively, slope, topographic position, pairing, and whether surface water was present. The solicitation resulted in the contribution of 18 datasets with 52 466 thaw depth measurements covering portions of the northern high-latitude permafrost zones in Canada, Russia, and the United States (Table 1, Fig. 1).

We screened the data for issues with units, sign convention, coordinates, and data type (e.g., factor, integer). Where we required categorical variables, we ensured these were spelled in a consistent manner and that the correct unique number of variables were returned. We mapped the data to check inaccurate site coordinates and checked discrepancies, such as missing negative signs from longitude, with contributors. We used histograms of measurement depths to identify any outliers in the data, several of which were removed after confirming with the contributors that they were the result of typographic errors. Data contributors were asked to note if any measurements hit rock, and, when noted, these observations were excluded from the final dataset.

2.2 Estimating active layer thickness

Over the course of the growing season, the depth of the thawing front increases as the active layer expands to its maximum. Therefore, measurements taken throughout the thaw season are not directly comparable with one another. Therefore, we standardized thaw depths taken at different times throughout the thawing season, which resulted in an estimated dataset of ALT. To do so, we estimated ALT using a modified version of the Stefan equation, used by Holloway and Lewkowicz (2020) and described by Riseborough et al. (2008) and Bonnaventure and Lamoureux (2013). Estimating ALT (Fig. 2) allows thaw depth measurements collected during different times in the growing season to be comparable and used to understand the full effects of wildfire on the active layer across paired sites in a given measurement year and for some of the sites across multiple years.

ALT was estimated based on air thawing degree days (TDD; i.e., days above 0 °C during the thawing season). Others have shown a correlation between TDD and ALT (e.g., Strand et al., 2021). Daily mean air temperatures were extracted from ERA5-Land daily aggregates (Muñoz Sabater, 2019) accessed through Google Earth Engine (Gorelick et al., 2017). Instrumental air temperature data are sparse across the northern high-latitude regions. We selected the ERA5-Land (Muñoz Sabater, 2019) dataset since it is available for the full region and time series, accessible through Google Earth Engine, and has been evaluated against meteorological station data (Rantanen et al., 2023; Clelland et al., 2024). Across the circum-Arctic and Asian boreal regions, ERA5-Land validation studies indicate a warming bias in winter months of 0.5 °C (Rantanen et al., 2023; Clelland et al., 2024), whereas validation studies in summer indicate a slight cooling trend of ~ 0.2 °C (Rantanen et al., 2023). Due to the scarcity of meteorological stations across the Northwest Territories, we provide additional validation for air temperature data from ERA5-Land using shielded air temperatures at a height of 1.5 m that were measured at six sites using Onset Corporation (USA) Hobo Pro U23-003 loggers (accuracy ± 0.21 °C;

Table 1. Brief description of the data contributions. The table includes the last name of the contributor, geographic location of the data, fire years that were sampled, a brief description of the sampling design and methods (see associated publications for additional detail), and relevant citations associated with the data.

Contributor	Country biome(s) – location description	Fire years	Sampling design and methods (see publications for additional details)	Citations
Baillargeon	United States tundra – Yukon–Kuskokwim Delta, AK, USA	1972, 2015	In 2018, thaw depth was sampled along 30 m transects at 1 m intervals. In 2019, thaw depth was measured along 30 m transects at 2 m intervals. We quantified depth to refusal with a tile probe.	Baillargeon et al. (2022)
Breen	United States tundra – Kougarok Fire Complex on the Seward Peninsula, AK, USA	1971, 1982, 2002, 2011	Thaw depth was measured in the four plot corners of 1 by 1 m unmarked plots along a chronosequence of time since fire and number of times burned ($n = 35$) and unburned ($n = 8$). Depth to refusal was measured with a tile probe. For each plot, the mean of the four depths is reported.	Hollingsworth et al. (2020, 2021)
Buma	United States boreal – central Alaska black spruce forest	2004/2005	Plots randomly placed in the four treatments: unburned, one fire in 2004/2005, two fires (1970s and 2004/2005), and three fires (1950s, 1970s, and 2004/2005). Thaw depth was sampled randomly within plots burned one to three times ($n = 5$ per plot, 33 plots), measured as depth to active layer at time of sampling (denoted as hitting frozen soil). The maximum depth of the probe was 1.8 m.	Hayes and Buma (2021) (design), Buma et al. (2022) unpublished data
Delcourt, Veraverbeke	Russia boreal – northeast Siberia, Russia	2018	In 2019, thaw depth was measured at five evenly spaced locations (every 7.5 m) along a 30 m transect centered within a 30 by 30 m plot. We measured depth to refusal using a pointed, graduated steel rod. Two measurements were taken 1 m apart at each location, totaling 10 measurements per plot.	Diaz et al. (2024), Delcourt et al. (2024)
Diaz	United States tundra – Alaska, USA	2022	Thaw depth was measured using a steel rod probe, which was inserted into the ground to the depth of resistance by the frozen ground. In 20 by 20 m plots, we performed measurements every 2 m. Measurements were taken in July–August, 1 year after the fire.	Lucas R. Diaz, Vrije Universiteit Amsterdam, unpublished data (2023)
Baltzer, Dieleman, Turetsky	Canada boreal – Northwest Territories, Canada	1940, 1960, 1969, 1971, 1972, 1973, 1980, 1981, 2011, 2013, 2014	From 2015–2019, thaw depths were measured using a tile probe at six locations evenly spaced along a 30 m transect centered within a 30 by 30 m plot. We quantified the depth to refusal.	Dieleman et al. (2022)
Douglas, Jorgenson	United States boreal – interior boreal near Fairbanks, AK, USA	2005–2020	Multiple transects were visited sporadically over the past 10 years. Thaw depths were measured by pushing a metal rod ("thaw probe") downward into the ground to refusal (Douglas et al., 2016). Repeat measurements were made at flags permanently installed in the ground or using a 100 m tape and high-resolution GPS measurements.	Douglas et al. (2016)
Frost	United States tundra – central Yukon–Kuskokwim Delta, western Alaska	1971, 1972, 1985, 2006, 2007, 2015	With the exception of 2015 burns, thaw depths were measured at 5 m intervals along three 30 m linear transects radiating at 120° intervals from the plot center, according to the US Bureau of Land Management's Assessment, Inventory, and Monitoring Program protocol (AIM; Toevs et al., 2011), providing 7 measurements per transect and 21 measurements per plot. For 2015 burns, plots consisted of four parallel 20 m transects oriented from east to west and spaced 5–10 m apart, following guidance from the Fire Effects Monitoring and Inventory System protocols; thaw depth was measured at 5, 10, and 15 m along each transect, providing 12 measurements per plot.	Frost et al. (2020)

Table 1. Continued.

Contributor	Country biome(s) – location description	Fire years	Sampling design and methods (see publications for additional details)	Citations
Gaglioti	United States tundra – the Noatak watershed, which drains the southwestern flank of the Brooks Range in northwestern Alaska	1972, 1984	Thaw depth was measured 2–3 m apart along 100 m long transects. We used a 1.5 m long tile probe and measured until depth of refusal.	Gaglioti et al. (2021)
Holloway	Canada boreal – Taiga Plains and Taiga Shield ecozones near Yellowknife, Canada	2014, 2015	Thaw depth was measured along 160 m transects with 52 measurement points per transect. At each point, a 1 cm diameter titanium probe was pushed into the ground until it met refusal.	Holloway et al. (2024)
Loranty	Russia tundra – northeastern Siberia larch forests	1972	Thaw depth measurements were taken at 1 m intervals along three 20 m transects across four burned sites within a single fire scar and four adjacent unburned locations. Thaw depth was quantified by measuring depth to refusal with a tile probe.	Loranty et al. (2014)
Manies	United States boreal – interior Alaska, black spruce forests	1999	Measurements within the black spruce sites occurred every 10 to 20 m along two linear transects within the site. These transects were laid out perpendicular to each other to negate any possible directional influences due to slope or dominant wind direction. Thaw depths were measured monthly.	Harden et al. (2006), Manies et al. (2004)
Natali	United States boreal and tundra – Bonanza Creek, Alaska USA; Anaktuvuk River fire, AK USA; Yukon–Kuskokwim Delta, AK	1983, 2003, 2004, 2007, 2015	For Hess Creek, thaw depths were measured at 1 m intervals along 1–3 m transects that measured 20–100 m across burned and unburned sites. For Bonanza Creek, thaw depths were measured along one to three transects of 20–100 m length every 1 m. For the Anatuvuk River fire, thaw depths were measured along a transect (Natali et al., 2018). For the Yukon–Kuskokwim Delta, thaw depths were measured across multiple sites across multiple years. We quantified the depth to refusal with a tile probe.	Natali et al. (2016, 2018), Natali (2018)
O'Donnell	United States boreal and tundra – interior boreal, AK, USA	1966, 1967, 1990, 2003, 2004	For Erickson Creek fire scar, three replicate thaw depth measurements across 10 plots per site type were taken (upland burned, upland unburned, lowland burned, lowland unburned) (O'Donnell et al., 2009). At Hess Creek and Taylor Highway sites, thaw depth measurements were made at one to five replicate plots per stand age (O'Donnell et al., 2011a, b, 2013). We quantified the depth to refusal with a tile probe.	O'Donnell et al. (2009, 2011a, b, 2013)
Olefeldt	Canada boreal – western boreal Canada	1964, 1967, 1975, 1982, 1984, 1995, 2000, 2006, 2007, 2008, 2012, 2013, 2014, 2019	At each site, we collected 100 thaw measurements in a 30 by 30 m grid, with measurement points every 3 m. We quantified the depth to refusal with a 150 cm steel probe.	Gibson et al. (2018)
Paulson, Alexander	Russia boreal – northeastern Siberia near Cherskiy, Russia, and Yakutsk, Russia	1983, 1984, 1990, 2001, 2002, 2003, 2010, 2015	Within each plot, we measured thaw depth five times along a 20 m south–north transect at 0, 5, 10, 15, and 20 m within each plot along one to three transects across 13 fire scars. We quantified the depth to refusal with a tile probe.	Alexander et al. (2020)
Rocha	United States tundra – North Slope of Alaska	1977, 1993, 2001, 2007	The CALM grid plus transects at 1–12-year-old sites (Rocha and Shaver, 2011) were measured, and transects only were measured at other sites. We quantified the depth to refusal with a tile probe.	Rocha and Shaver (2011)
Sizov	Russia tundra – northwestern Russia, Nadym region of the Yamal–Nenets Autonomous Okrug	2020	Across seven sites, temperature was measured in shallow boreholes with a Tr 46908 thermometer (TR di Turoni & c. Snc, Italy) and drilling was carried out using a handheld motor-drill Stihl BT 360 (Stihl, Germany). Measurements occurred in mid-August, at approximately 10 cm increments.	Sizov et al. (2020)

Figure 1. Map of the northern high-latitude permafrost zone showing the percent of thaw depth measurements by ecozone (circle color; Dinerstein et al., 2017) with the extent of continuous, discontinuous, and sporadic permafrost shown in shades of blue (Brown et al., 1998). Points are sized and labeled with the percent of measurements within each ecozone. The Arctic Circle is shown with the thick dashed black line.

precision ± 0.02 °C). All air temperature data were aggregated from 2 h samples to daily averages and sites included thaw depth measurements (Holloway, 2020). We calculate Pearson's correlation coefficient (R), bias (defined as the summation of modeled minus measured divided by the number of data points), and the root mean square error (RMSE). The correlation is ∼ 0.99, with a warming bias of 0.54 °C and an RMSE of 2.23 °C (Fig. S1 in the Supplement).

First, we defined the end of the thaw season for each measurement location and year based on when the 5 d mean daily air temperature shifted from above to below freezing. We then subtracted 14 d from the end-of-season date to account for the lag between surface freezing and the refreezing of the bottom of the active layer. Typically, the active layer begins to freeze upward while the air temperature is still above zero, requiring approximately 7–14 d until the surface freezes (Osterkamp and Burn, 2002). Following the Stefan equation (Freitag and McFadden, 1997), we calculate A as the square root of the sum of daily mean air temperature TDD prior to the day of year of the field measurement (i.e., thaw depth), as in Eq. (1):

$$A = \sqrt{\sum_{\text{TDD thaw depth}=1}^{n} \text{TDD thaw depth}}. \quad (1)$$

We calculate B as the square root of the sum of daily mean air temperature TDD (i.e., days above 0 °C) prior to the end of the thaw-season day of year (i.e., ALT) in Eq. (2):

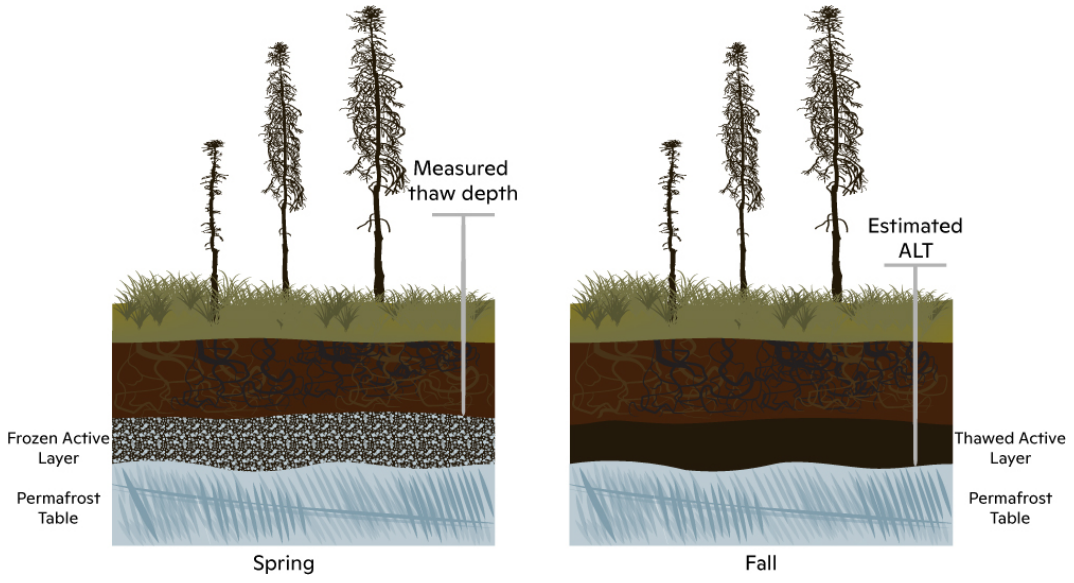

Figure 2. Diagram of early-season thaw depth measurement versus late-season active layer thickness. The active layer expands during the thawing season, reaching its maximum thickness between August and November depending on the location.

Table 2. An example of estimating ALT using Eqs. (1)–(3) from two in situ thaw depth measurements at two sites (A and B) using the same data as in Fig. 3.

	Site	A	B
Data contribution	Timing of measurement	Early season	End of season
	Year	2015	2015
	Month	6	9
	Day	10	11
	Day of year	161	254
	Measurement depth (cm)	34	127
Calculated from ERA5 data extracted based on location	Day of year first of 5 consecutive days at zero	299	299
	Day of year to estimate ALT	285	285
	Eq. (1)	25.25	45.95
	Eq. (2)	48.03	48.03
Estimated ALT	Eq. (3) (cm)	65	133

$$B = \sqrt{\sum_{\text{TDD ALT}=1}^{n} \text{TDD ALT}}. \quad (2)$$

Finally, we multiplied the field-measured depth by the ratio of the first two equations to calculate the estimated ALT in Eq. (3):

$$\text{estimated ALT} = \text{field-measured depth} \times (B \div A). \quad (3)$$

An example of the calculation for two sites is provided in Table 2 and shown in Fig. 3.

Estimates were excluded for observations that hit rock, were greater than the depth of the measurement probe, or were missing the day of month (Table S2). We were unable to convert every early-season thaw depth to ALT if the date of measurement was not preceded by at least 1 d above 0 °C, in which case these measurements were removed from the estimated dataset. Ultimately, 48 669 of the original 52 466 measurements were included in the estimated dataset.

2.3 Quantify uncertainty of estimated ALT

We quantify uncertainty in our estimates of ALT by calculating Pearson's correlation coefficient (R), bias (defined as the summation of modeled minus measured values), and RMSE. The bias indicates whether estimated ALT is over- or underestimated, while the RMSE provides an average error regardless of sign. We used two datasets for this analysis from contributors that had repeat measurements from within a season for the early/mid-season and late season at the same locations. These datasets differed as one was a subset of their

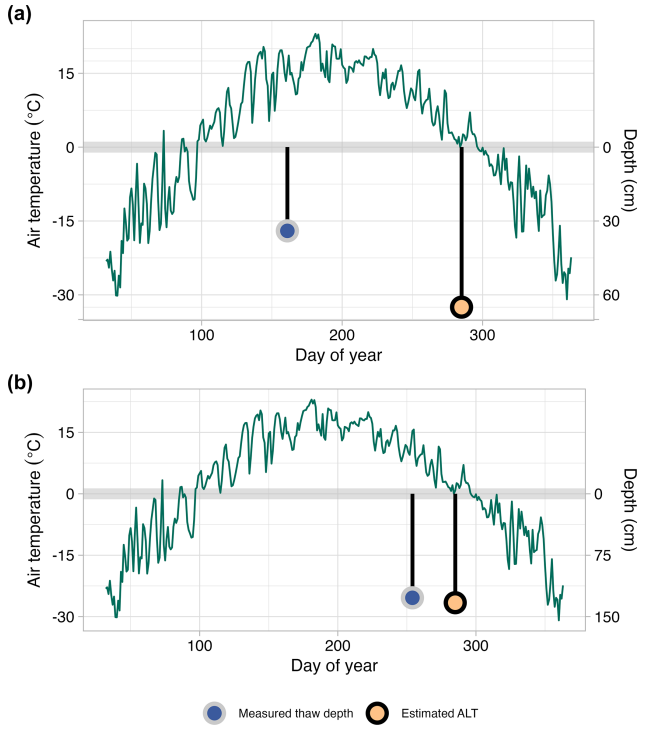

Figure 3. An example of estimating active layer thickness from two in situ thaw depth measurements using seasonal air temperature. Air temperature through the thawing season (green line) is shown for two separate sites, one with an early-season thaw depth measurement **(a)** and a second with an end-of-season thaw depth measurement **(b)**. For each site, we show the measured thaw depth (blue point) and estimated ALT depth (orange point) for the day of year either measured or estimated. The right y axis shows thaw depth (cm), the left y axis shows air temperature, and the x axis shows the day of the year.

data contributed to the data synthesis for the boreal near Yellowknife, Canada ($N = 626$; Holloway et al., 2024), whereas the other was used solely for quantifying uncertainty for tundra on the Seward Peninsula, AK ($N = 37$; Breen, unpublished). The tundra data were missing key metadata, which precluded them from being used in the synthesis. We used the early/mid-season measurements to estimate thaw depths for the date of the late-season measurement (as opposed to the end of the thaw season defined using ERA5-Land) following the methodology described in Sect. 2.2 to quantify the uncertainty in the estimation process.

2.4 Spatial attributes

We added spatial attributes to the data through spatial joins. We generated a point shapefile using the latitude and longitude coordinates with the coordinate reference system (CRS) 4326 (i.e., WGS 84). We performed a spatial join to add ecozone data (Dinerstein et al., 2017), retaining the ecozone and biome names. We then performed a second spatial join with permafrost data (Brown et al., 1998), retaining permafrost extent (e.g., continuous, discontinuous, sporadic). We show the distribution of estimated ALT measurements by ecozone (Fig. 4). The spatial coverage, and hence inherent resolution, of these polygon products is much larger than the data points or any site-level aggregation. Due to the coarser resolution, data contributors' designation of biome outweighed what was assigned through the spatial join. The small percentage of plots where the biome was misassigned were visually inspected, found to be adjacent to the boundary with the matching biome, and manually reassigned (see the "Data availability" section).

2.5 Data structure and columns

The resulting dataset includes 32 attributes including attributes from the initial contribution, plus the attributes from the spatial joins and the derived ALT estimates all described in Table 3. The dataset is shared in comma-separated value (.csv) format with 48 669 rows and 32 columns. For missing values, we used NA and −9999 for character and numeric fields, respectively.

2.6 Aggregating plot-level means and burned to unburned pairs

While the main objective of the data synthesis is to provide paired burned–unburned ALT estimates, we also want to provide details on aggregating to the site/plot level. We aggregated plot- and paired-level data in R with "tidyverse" (Wickham et al., 2019). Plot-level data were aggregated using the "group_by" function using the following variables: data contributor ("submitNm"), burned or unburned ("distur"), site-level identifier ("siteId"), plot-level identifier ("plotId"), fire year ("fireYr"), and year of measurement ("year"), which captures both the spatial and temporal component of the data. We then calculated the mean ALT for each plot that includes 28 attributes (see Table 3 for descriptions). Paired burned and unburned sites are a unique and defining characteristic of this dataset. Data contributors were required to provide details on how their burned measurements paired with unburned measurements. Characteristics of unburned plots were required to be representative of biogeoclimatic conditions pre-fire and within close proximity to their paired burned plot(s). The dataset includes a code to link burned with unburned sites ("paired"). To aggregate at the paired level, we grouped by data contributor ("submitNm"), burned or unburned ("distur"), pairing code ("paired"), and year of the fire event ("fireYr"), and these can be further grouped by time since fire ("tsf"). The paired burned–unburned data include 13 attributes (Table 3).

Table 3. Description of data attributes and data format. All attributes are included with the raw data. Attributes included with the plot-level data are denoted with [1] and attributes included with paired burned–unburned are denoted with [2].

Attribute	Format	Description
plotId[1]	character	A unique identifier assigned by the data contributor to identify the field plot.
siteId[1]	character	Site name assigned by the data contributor specific to the fieldwork.
lastNm[1,2]	character	Last name(s) of the person(s) contributing the data provided by the data contributor.
submitNm[1,2]	character	Last name of the data contributor that submitted the form (single name only).
biome[1,2]	character	Boreal (B) or tundra (T) assigned by the data contributor.
hline distur[1,2]	character	Categorical variable to identify location as burned or unburned provided by the data contributor.
cntryId[1,2]	character	Dropdown list of two-digit code: Russia (RU), USA (US), Canada (CA), Finland (FI), Norway (NO), Sweden (SE), Iceland (IS), Greenland (GL) assigned by the data contributor.
fireYr[1,2]	integer	Four-digit year of when the fire event occurred provided by the data contributor.
fireId[1,2]	character	Unique fire event identifier assigned by the data contributor.
gtProbe[1]	character	Permafrost thaw depth exceeds (i.e., greater than, gt) the length of probe, yes (y) or no (n), provided by the data contributor.
hitRock[1]	character	Probe hit rock, yes (y) or no (n), provided by the data contributor.
lat[1]	float	Latitude in decimal degrees in WGS 84 provided by the data contributor.
lon[1]	float	Longitude in decimal degrees in WGS 84 provided by the data contributor.
year[1,2]	integer	Four-digit year the data were collected provided by the data contributor.
month	integer	Two-digit month (values 01–12 accepted) the data were collected provided by the data contributor.
day	integer	Day of month data were collected values (1–31) provided by the data contributor.
orgDpth[1]	integer	Organic layer thickness measured from the ground/moss surface to the organic-mineral interface, as a site mean in centimeters, provided by the data contributor.
srfH2O[1]	character	A categorical variable describing if plot locations experience seasonal inundation (i.e., standing surface water during the early season but dry by late season). Seasonal inundation (Y: yes), no seasonal inundation (N: no), or unknown (U). Provided by the data contributor.
msrType	character	A categorical variable of thaw (T) or active (A). Active refers to active layer thickness (i.e., maximum seasonal thaw at the end of growing season), and thaw refers to thaw depth (i.e., less than seasonal maximum taken earlier than the end of thawing season). Provided by the data contributor.
msrDoy	integer	Day of year (DOY) for the day of measurement converted from YYYY-MM-DD.
msrDepth	float	The field measurement of the thaw depth or ALT in centimeters. Provided by the data contributor.
topoPos[1]	character	Categorical variable describing the topographic position of plot locations as upland (U), midslope (M), or lowland (L). Provided by the data contributor.
slope[1]	character	Categorical variable describing slope as "flat" or "sloped" provided by the data contributor.
vegCvr[1]	character	Evergreen needleleaf (EN), broadleaf deciduous (BD), deciduous needleleaf (DN), mixed needleleaf majority MNM, mixed (M), mixed broadleaf majority (MBM), barren (B), graminoid tussock-dominated (GT), graminoid non-tussock-dominated (GNT), prostrate-shrub-dominated (P), erect-shrub-dominated (S), and wetlands (W). Provided by the data contributor.
resBiome[1]	character	Biome assigned by spatial join with the Resolve data product (vector data) "BIOME_NAME" (Dinerstein et al., 2017).
resName[1]	character	Ecozone name assigned by spatial join with the Resolve data product (vector data) "ECO_NAME" (Dinerstein et al., 2017).

Table 3. Continued.

Attribute	Format	Description
permaExtent[1,2]	character	Permafrost extent (vector data) assigned by spatial join with the permafrost ground-ice map "EXTENT" as C: continuous, D: discontinuous, or S: sporadic (Brown et al., 1998).
estDoy[1]	integer	The day of year used to estimate ALT based on when the 5 d mean daily air temperature shifted from above to below freezing.
estDepth[1,2]	float	The estimated ALT in centimeters; calculated using air temperature from ERA5-Land and field-measured thaw depth.
paired[1,2]	character	Identifying code to pair unburned measurements to burned measurements provided by the data contributor.
tsf[1,2]	integer	Time since fire calculated by subtracting year from fireYr.
tsfClass[1,2]	character	Binned time since fire (tsf) classes in years as "unburned", 0–3, 4–10, 11–20, 21–40, or > 40.
n[1,2]	integer	Number of measurements used to calculate plot-level or paired burned–unburned means.

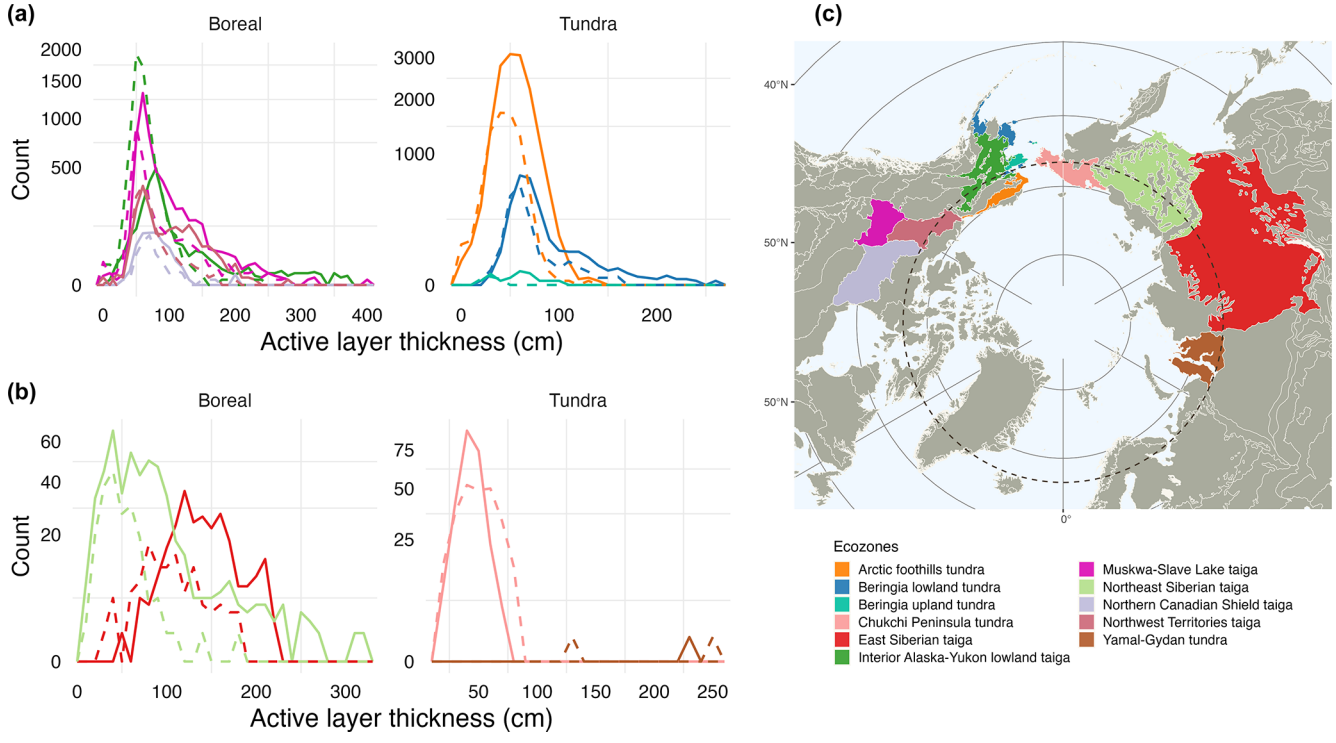

Figure 4. Frequency distribution graphs showing estimated active layer thickness (cm) by ecozone split by North America **(a)** and Eurasia **(b)**, with a solid line for burned distribution and dashed line for unburned distribution. Map of ecozones for location reference **(c)** (Dinerstein et al., 2017). The *y* axis is the count of measurements and the *x* axis is the depth in centimeters. Both the *x* and *y* axes vary by panel and *y* axes are adjusted to show low counts.

3 Data summary

3.1 General characteristics of the data

In total, the final dataset includes 48 669 observations from the original 52 466 observations across 9446 plots and 388 sites. Thaw depth measurements are predominantly from North America, with 35 272 (19 739 burned, 15 533 unburned) in Alaska and 11 844 (7553 burned, 4291 unburned) in Canada, as well as 1553 (998 burned, 555 unburned) in Russia. These in situ measurements were collected within the continuous, discontinuous, and sporadic permafrost zones (Fig. 1). Data were contributed with both burned and unburned paired sites with fire years ranging from 1900

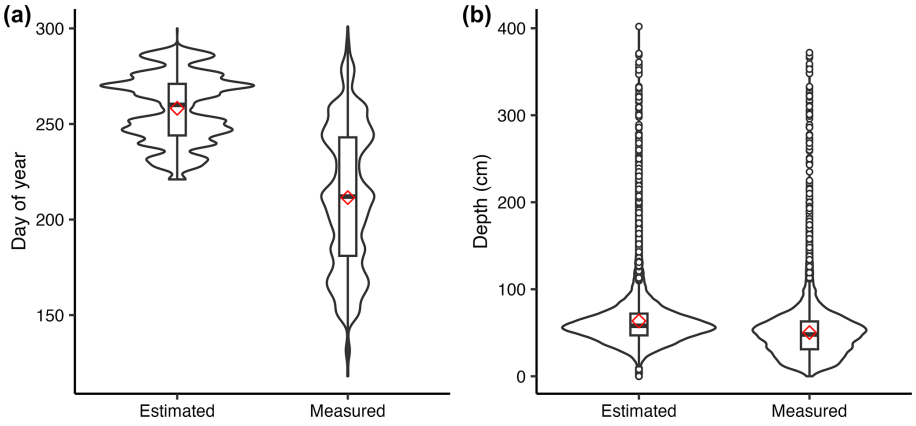

Figure 5. The distribution for in situ measurements vs. estimated measurements. For day of year **(a)** and thaw depth **(b)**, we show the distribution for in situ measurements vs. estimated measurements using violin plots overlain with box plots, with a red diamond marking the mean. Measured day of year and depths were provided in the raw data contribution. The day of year shows a wide spread of dates, which is caused by the broad geographic extent of the data. Estimated values were calculated to create a dataset that characterizes maximum thaw depth (i.e., ALT).

to 2022 across 112 fire events. There are 193 unique paired burned–unburned measures based on pair ID (76), fire year (37 unique years), fire events (63 unique events), and time since fire spread across 11 ecozones. There are 21 589 estimated observations across the boreal forests/-taiga and 27 080 estimated observations across the tundra biomes (Fig. 4). There are 27 638 observations from continuous permafrost, 12 905 from discontinuous permafrost, and 8126 from sporadic permafrost.

3.2 Estimated ALT

The estimated ALT provides a temporally consistent measurement capable of quantifying the effects of wildfire on active layer dynamics temporally and spatially. The data show the shift from measured thaw depth to estimated ALT characterized by a narrower range of dates and depth measurements (Fig. 5a and b). The day of year is condensed for the estimated measures (Fig. 5a), which was anticipated since the contributed data were collected throughout the thawing season, resulting in a wide spread due to the broad geographic extent of the data, whereas the estimated data were truncated to the later part of the thaw season, resulting in a narrow range of days. The uncertainty in the estimated ALT varies with biome and disturbance (Table 4, Fig. 6). Boreal burned values tend to be underestimated by about 5 %, whereas unburned values tend to be overestimated by about 15 %. For the tundra, burned and unburned values tend to be overestimated by 19.6 % and 22.8 %, respectively. The sample size is much smaller for the tundra biome for estimating uncertainty.

Table 4. Quantifying uncertainty for estimated ALT. We report the root mean square error (RMSE), percent uncertainty, mean residual error as an indication of bias, and sample size for burned and unburned sites in the validation dataset. Negative values indicate an overestimation and positive values indicate an underestimation.

Biome	Disturbance	RMSE	Percent uncertainty	Mean residual error (bias)	Sample size
Boreal	Burned	22.8	4.6	5.7	413
Boreal	Unburned	20.3	14.5	−8.4	212
Tundra	Burned	29.2	19.6	13.9	20
Tundra	Unburned	5.6	22.8	12.5	6

3.3 Difference in estimated ALT between burned and unburned sites

By aggregating the burned and unburned pairings, we show the percent difference in estimated ALT between burned and unburned sites post-fire (Figs. 7 and S3). Most sites show a thickening of the active layer post-fire compared to nearby unburned sites. Generally, across boreal sites the mean percent difference shows a thickening of the active layer in the 2 decades following fire, followed by a recovery in the subsequent decades (e.g., time since fire 21–40 and > 40). The magnitude of difference varies by biome and permafrost extent. In the boreal forest continuous permafrost region, the means follow this general trend of expansion followed by recovery; however, there are very limited and no data at 4–10 and > 40 years, respectively. The boreal forest discontinuous permafrost region follows the general trend, whereas the boreal forest sporadic permafrost region shows a lower percent difference in the 2 decades following fire where the active layer does expand but not to the same extent as seen in

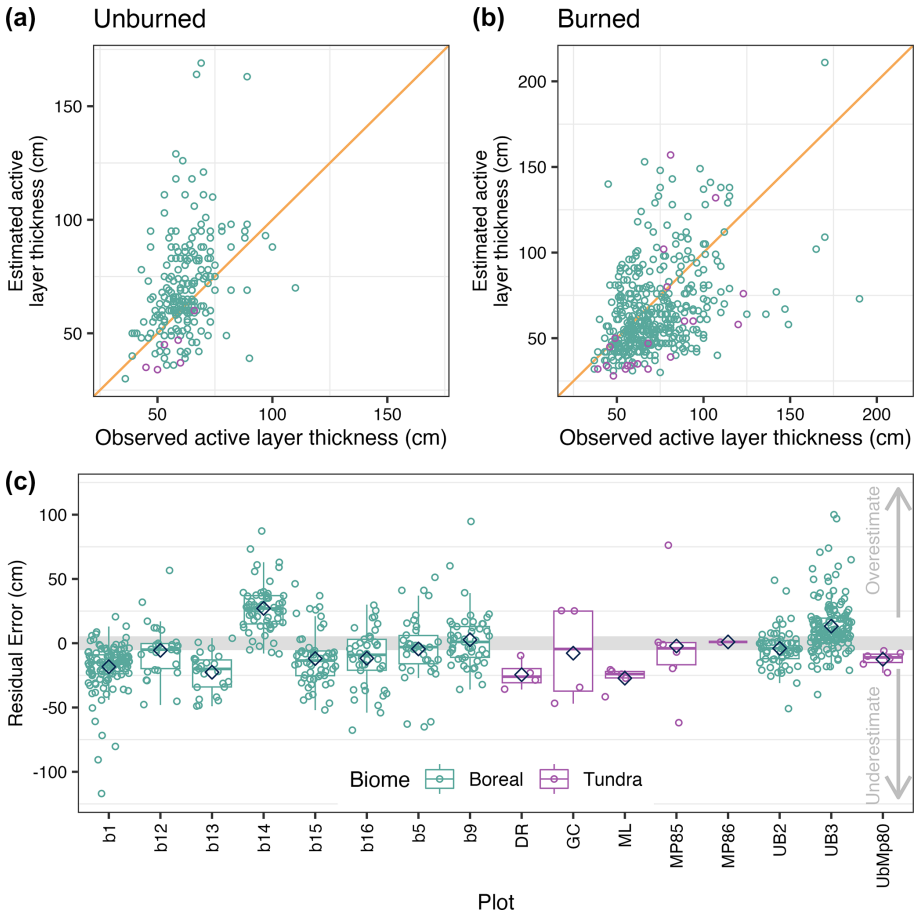

Figure 6. Quantifying uncertainty of ALT estimates. Panels **(a)** and **(b)** show observed depths compared to estimated depths split by unburned and burned plots, with the orange line showing a slope of 1. Panel **(c)** shows the bias by plot identifier, where zero indicates no difference between the observed and estimated values. Negative values indicate an underestimation and positive values indicate an overestimation, with the mean shown by the blue diamond. Burned sites include b1, b12, b13, b14, b15, b16, b5, b9, DR, GC, ML, MP85, and MP86, and unburned sites are ub2, ub3, and UbMp80.

the continuous or discontinuous permafrost following a varied recovery at 21–40 and > 40 years. The tundra biome follows the same general trend that the boreal sites do where mean percent difference shows a thickening of the active layer in the 2 decades following fire, followed by a recovery in the subsequent decades (e.g., time since fire 21–40 and > 40). This trend is most distinct for tundra sites with continuous permafrost, whereas sites with discontinuous permafrost show a bit more variability for 11–20, 21–40, and > 40 years. The tundra sites with discontinuous permafrost have a sample of one for 21–40 and > 40 years, which makes it challenging to fully understand the recovery trend. The trend of post-fire thickening of the active layer followed by recovery illustrates the effect of climate on permafrost recovery. The variability in the extent of the thickening of the active layer across permafrost zones might provide insight into potential future patterns. Specifically, the reduced thickening seen in the warmer boreal sporadic region might be a future pattern that we see extending to the boreal discontinuous zone as the climate continues to warm.

4 Strengths, limitations, and opportunities

4.1 Strengths

The FireALT dataset (Talucci et al., 2024) offers paired burned and unburned sites that can be aggregated and viewed both spatially and temporally to provide critical insights for understanding wildfire impacts on ALT, a feature commonly used to determine permafrost conditions. Field data collection is often spatially and temporally opportunistic, making comparisons of disparate datasets difficult. For example, several geographically similar sites had depth measurements collected across a wide range of dates throughout August and September, but these measurements do not necessarily capture the maximum ALT and are therefore not comparable. Further, it is challenging to compare early-season

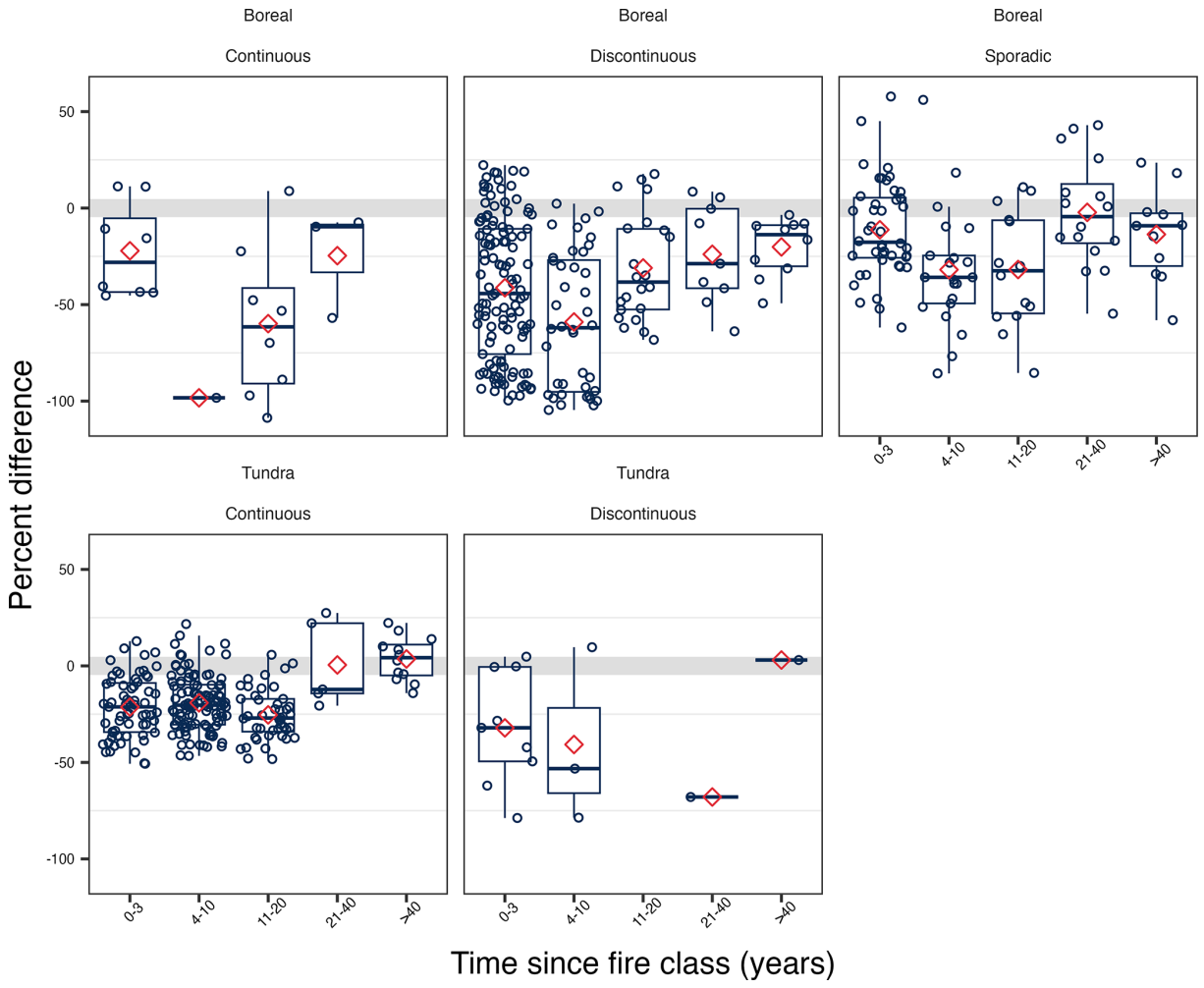

Figure 7. Percent difference in estimated ALT between burned and unburned paired sites in the years following wildfire. The percent difference is calculated as (unburned-burned)/((unburned + burned)/2) × 100. Negative values indicate that the burned sites have a thicker active layer than the unburned site, while values around zero show little difference in ALT, and positive values indicate that unburned sites have a thicker active layer than the burned ALT. The red diamond indicates the mean based on paired burned–unburned sites, which are then aggregated by time since fire class, permafrost extent, and biome. The box and whisker plots show the split in quantiles. See the Supplement to see a similar plot by ecozone (Fig. S2).

to end-of-season thaw depth measurements (Holloway and Lewkowicz, 2020). By estimating ALT, the data can be used to extrapolate beyond individual measurements and provide a broader understanding of spatial and temporal feedbacks between wildfires, permafrost, and climate. Additionally, data include several environment attributes, e.g., organic layer depth, slope, topographic position, and whether surface water was present. Future analyses could integrate these environment variables to expound upon the relationship between the environment, ALT, and wildfire. Finally, we show a general expansion of the active layer after fire followed by recovery 40 years post-fire, but the magnitude of expansion and recovery vary by biome and permafrost zone, pointing to the role of vegetation, permafrost conditions, and climate in active layer dynamics in response to wildfire (Brown et al., 2015). Climate has changed over the time period of the fire events captured within this dataset. Generally, the data indicate that we may expect the active layer to fully recover 40 years post-fire, but that may change for more recent fires. The boreal sporadic zone experiences less expansion of the active layer with a less distinct recovery, which demonstrates how climate influences active layer recovery in warmer regions. This illustrates how climate influences permafrost recovery, and with a warming climate, we may expect to see patterns more like this in boreal discontinuous permafrost zones.

4.2 Limitations, uncertainty, and bias

Estimating ALT is crucial for spatial–temporal evaluations of wildfire–permafrost interactions due to the variability in

thaw depth throughout the thaw season. However, uncertainties arise in the estimated ALT from the data we integrate to make those calculations. Air temperature can be a reliable metric for calculating maximum ALT (Osterkamp and Burn, 2002; Holloway and Lewkowicz, 2020), but the coarse-resolution climate data and in situ weather station gaps (Clelland et al., 2024), as well as the lack of accounting for disturbance effects on air temperature (Kurylyk and Hayashi, 2016; Muñoz-Sabater et al., 2021; Helbig et al., 2024), all impact the accuracy of the estimated ALT. The Stefan equation assumes negligible soil heat capacity and can thus overestimate thaw depth, and it also does not account for fire altering the surface energy balance (e.g., reducing albedo, loss of canopy and shading) and heat fluxes (e.g., loss of aboveground biomass), all of which increase thaw depths and can contribute to underestimations of ALT (Kurylyk and Hayashi, 2016). Our quantification of uncertainty supports this underestimation bias for burned sites and overestimation for unburned sites in the boreal biome. Further, the lack of inclusion of frozen water content in the Stefan equation may affect early-season measurements due to the zero curtain, where the rate of thawing may not scale directly with air temperature (Osterkamp, 1987; Romanovsky and Osterkamp, 2000). These effects likely vary between tundra and boreal sites. These are dynamic systems with multiple feedbacks that influence the freeze–thaw cycle and the timing of maximum thaw depth. Similarly, the time at which permafrost begins to refreeze from the bottom varies with permafrost temperature, soil moisture and thermal properties, and local edaphic hydrological conditions. Consequently, our assumption that ALT occurs 14 d before the date at which air temperature drops below freezing is another source of uncertainty. Overall, interannual variability in ALT is dependent on complex interactions between air temperature, precipitation, snow dynamics, hydrothermal processes, water energy exchanges, and fluctuations in thaw-season length, which are a source of uncertainty in our approach (Shur et al., 2005; Hu et al., 2023; Grünberg et al., 2024). At warmer boreal sites the 14 d lag may be longer or nonexistent depending on the complex interactions of these landscape-level controls. Despite this, estimating ALT allows for insightful comparisons between sites that are not appropriate or meaningful with the raw data.

Burn severity is a critical component of wildfire that impacts ALT and permafrost stability through combustion of the insulating organic matter, vegetation, and post-fire changes in albedo (Rocha and Shaver, 2011; Alexander et al., 2018). We do not account for burn severity in the data, which could strongly influence differences we see between burned and unburned ALT. Burn severity could be estimated using the organic depth measurement in the data, but the organic depth will be influenced by time since fire or through the integration of satellite imagery that could be used as a proxy for burn severity. However, vegetation indices that estimate burn severity (e.g., differenced normalized burn ratio – dNBR) are typically better correlated with aboveground burn severity but less indicative of burn depth (e.g., Delcourt et al., 2021). Recent research which has shown combinations of remote sensing proxies, dNBR, and land surface temperature could be used in conjunction with these field measurements to estimate changes in ALT across fire scars (Diaz et al., 2024). Additionally, the ice content of permafrost may impact the interaction between wildfire and permafrost, with direct effects on ALT, particularly where subsidence is involved or where the increase in ALT contributes to the degradation of ice-rich permafrost (e.g., Yedoma) in the short term (Nelson et al., 2021; Strauss et al., 2021; Jones et al., 2024). Subsidence is not accounted for in the synthesized data. Subsidence can introduce additional bias in the measurement of ALT since thaw depth probing uses the surface as a reference. In areas where subsidence occurred after fire, our dataset will underestimate the magnitude of active layer thickening caused by fire. Bias from subsidence is difficult to estimate because it would be spatially heterogeneous, temporarily nonlinear, and largely dependent on ice content (Shiklomanov et al., 2010; O'Neill et al., 2023; Painter et al., 2023).

In addition to these physical controls, there are additional biogeomorphic factors that influence changes in ALT from fire. Landscape-scale variation in topography, soil type and moisture, ground ice content, and vegetation cover and regrowth are all sources of uncertainty that cannot be accounted for in our synthesized dataset (Shiklomanov et al., 2010; O'Neill et al., 2023; Painter et al., 2023). Accounting for these drivers would require datasets that may or may not be available and is a separate research effort outside the scope of this paper. We use ecozones to highlight summary statistics of the dataset since ecozones are characterized by sharing similar climates, geologic substrates, vegetation, and landforms. The use of ecozones provides a broad overview of the data, which captures some of the variability in ALT measurements; however, finer-scale landscape features likely still add substantial variation to the estimated ALT and changes from fire. Future work could analyze how microtopographic features that influence local hydrology, burn severity, vegetation structure and function, and ice content impact wildfire-induced changes in ALT. Further, while growing season lengths and thawing degree days have increased over the last century (e.g., Barichivich et al., 2012), the data synthesized here were only measured from 2001 onward despite covering fire events from 1900–2022. Recent thaw depth measurements from areas that burned more than several decades ago represent a post-fire evolution of the active layer under climatic conditions that no longer exist. The snapshot of thaw depth related to wildfire events in space and time provided by this dataset may therefore include climatic effects that are hard to disentangle under current warming trends (e.g., Liu et al., 2024), which may bias the estimated ALT.

4.3 Representativeness of the data

The data included in our dataset are predominantly from North America, and there are large spatial gaps across the northern high-latitude permafrost region (Fig. S3). For example, Russia is underrepresented despite containing 65 % of the northern high-latitude permafrost (Anisimov and Reneva, 2006; Streletskiy et al., 2019) and a majority of the burned area within the northern permafrost region (Loranty et al., 2016). The lack of data for this region is further exacerbated by the Russian invasion of Ukraine (López-Blanco et al., 2024), which has impacted international collaborations. Additionally, some of the spatial gaps could be a function of the submission criteria that required a burned–unburned pair. Due to the remoteness of northern high-latitude fires, field campaigns may be constrained spatially and temporally based on accessibility of field sites and timing of field campaigns. Opportunistic site selection introduces bias into the dataset; however, this is unavoidable for a data synthesis effort that relies on contributions of existing data.

4.4 Future research opportunities

There is an opportunity to expand this dataset to increase the spatiotemporal coverage of the data to better understand impacts of wildfire on permafrost dynamics. While we touch on how ALT differs across burned and unburned sites across the northern high-latitude permafrost zone, further investigation is warranted on the role of wildfire in permafrost dynamics. We have identified several understudied research areas that could be augmented with this dataset. First, the dataset could be used to further investigate the geospatial distribution of permafrost recovery following fire across the northern high-latitude permafrost zone. Second, these data could be used to determine the probability (i.e., likelihood) of permafrost recovery after wildfire as a function of ecotype or ecoclimatic zone, permafrost classification, fire rotation period, and/or climate. Third, the data could aid in determining the soil C consequences of temporary or permanent post-fire permafrost degradation. Fourth, investigations could be structured to identify changes in wildfire activity that affect the likelihood of permafrost recovery/degradation and associated soil C vulnerability using predictive mapping. Fifth, the data could be used to develop an organic layer deficit value that would represent the difference between the organic layer thickness in the burn scar and the organic layer thickness at the unburned control site. Sixth, this dataset could be augmented with quantification of subsidence and the combination of that with ALT to understand how much new permafrost is exposed to seasonal thaw as a result of fire. Finally, there is the opportunity for this dataset to be used in algorithm development, calibration, and validation for evolving process-based models that are trying to capture the impact of fires on permafrost.

5 Data availability

The FireALT dataset (https://doi.org/10.18739/A2RN3092P, Talucci et al., 2024) is publicly available for download through the Arctic Data Center under a Creative Commons Attribution 4.0 International copyright (CC BY 4.0). Data should be appropriately referenced by citing this paper and the dataset (see Arctic Data Center). Users of the data are invited to ask questions by contacting the dataset developers. We recommend that researchers planning to use these data as a core portion of their analysis collaborate with the data developers and relevant individual site contributors. The data are available for download as a .csv file through the Arctic Data Center (https://doi.org/10.18739/A2RN3092P, Talucci et al., 2024).

6 Conclusions

The FireALT dataset offers a collection of paired burned and unburned plots with measured thaw depths and estimated ALT. By estimating ALT, we address a key challenge: the ability to assess impacts of wildfire on ALT when measurements are taken at various times throughout the thaw season depending on the time of field campaigns (typically June through August). This dataset can be utilized for future research activities that can expand understanding of the feedbacks between permafrost, wildfire, and global climate systems. Changes to the active layer serve as an important diagnostic indicator that requires continuous monitoring under the current dynamic climate conditions to further understand temporary or permanent changes to permafrost and subsequent losses in carbon storage. These types of data synthesis efforts are crucial for addressing understudied research areas, particularly algorithm development, calibration, and validation for evolving process-based models as well as extrapolating across space and time, which will elucidate permafrost–wildfire interactions under accelerated warming across the high-northern-latitude permafrost zone.

Supplement. The supplement related to this article is available online at https://doi.org/10.5194/essd-17-2887-2025-supplement.

Author contributions. The FireALT dataset was conceptualized during the 2019 Permafrost Carbon Network meeting by ACT, BMR, DO, KLM, LTB, MAW, MJL, and MML with additional input by ACT, AKP, AVR, BMR, JAO, JEH, KLM, LTB, MAW, MJL, MRT, NB, REH, SMN, and SV for the methods. Data curation was carried out by AB, ACT, AKP, AS, AVR, BB, BVG, CJFD, CM, CMD, DO, GVF, HDA, JAO, JEH, JLB, KLM, LB, LBS, LRD, LTB, MCM, MML, MRT, MTJ, NB, OS, RAL, REH, SMN, SS, SV, TAD, TAS, and TH. Formal analysis was performed by ACT, JEH, and MML. ACT and MML provided project management. BMR and MML provided supervision. Visualizations were created by ACT, JEH, and JD. ACT, JEH, and MML wrote the origi-

nal draft. All authors contributed to the realization of the permafrost wildfire dataset and participated in the editing of the paper.

Competing interests. At least one of the (co-)authors is a member of the editorial board of *Earth System Science Data*. The peer-review process was guided by an independent editor, and the authors also have no other competing interests to declare.

Disclaimer. Any use of trade, firm, or product names is for descriptive purposes only and does not imply endorsement by the US Government.

Publisher's note: Copernicus Publications remains neutral with regard to jurisdictional claims made in the text, published maps, institutional affiliations, or any other geographical representation in this paper. While Copernicus Publications makes every effort to include appropriate place names, the final responsibility lies with the authors.

Acknowledgements. Anna C. Talucci acknowledges Christina Shintani and Greg Fiske at Woodwell Climate Research Center for their cartographic feedback and recognizes funding support from NSF Arctic System Science (award no. 2116864), the NASA Arctic Boreal Vulnerability Experiment (grant no. 80NSSC22K1244), the NSF (award no. 2019485), and NSF OPP-1708322. Jean E. Holloway acknowledges Antoni Lewkowicz at the University of Ottawa for the support for field data collections. Michael M. Loranty recognizes funding support from NSF OPP-1708322 and from the Colgate University Research Council. Brendan M. Rogers recognizes support from the Gordon and Betty Moore Foundation (grant no. 8414), NSF Arctic System Science (award no. 2116864), the NASA Arctic Boreal Vulnerability Experiment (grant no. 80NSSC22K1244), the NSF (award no. 2019485), and funding catalyzed by the Audacious Project (Permafrost Pathways). Amy Breen acknowledges Colette Brown, Fernanda Santos, and Thomas Moran for assistance in the field and funding from the Director, Office of Science, Office of Biological and Environmental Research of the US Department of Energy under contract no. DE-AC02-05CH11231 as part of the Next-Generation Ecosystem Experiments (NGEE Arctic) project. Jonathan A. O'Donnell acknowledges Jennifer Harden and support from the US Geological Survey for field data collections. David Olefeldt acknowledges Carolyn Gibson for her fieldwork contributions to the contributed data. Logan T. Berner was supported by the NASA Arctic Boreal Vulnerability Experiment (80NSSC22K1244 and 80NSSC22K1247). Susan M. Natali acknowledges John Wood and the Polaris Project team for field support and funding from the NSF (1417700, 1915307, 1561437) and NASA (NNX15AT81A). Thomas A. Douglas acknowledges the US Department of Defense's Strategic Environmental Research and Development Program (Project RC18-1170) and Environmental Science and Technology Certification Program (Project RC22-D3-7408) as well as the US Army Engineer Research and Development Center Basic Research Portfolio through Program Element PE 0601102A/T14/ST1409. Seeta Sistla and Natalie Baillargeon acknowledge support from NSF 2218742. Jennifer L. Baltzer acknowledges funding through the Government of the Northwest Territories' Cumulative Impacts Monitoring Program Project 170, Canada First Research Excellence Fund's Global Water Futures program (project Northern Water Futures), the Natural Sciences and Engineering Research Council's Discovery Grant funding, and the Canada Research Chairs program. Data collection was conducted under Aurora Research Institute's scientific research license numbers 16815, 16755, 16311, 16018, 15879, and 15609. Clement J. F. Delcourt acknowledges funding from the Dutch Research Council (NWO) through a Vidi grant (grant no. 016.Vidi.189.070) and from the European Research Council (ERC) through a Consolidator grant under the European Union's Horizon 2020 research and innovation program (grant no. 101000987), both awarded to Sander Veraverbeke. Tatiana A. Shestakova acknowledges funding from the Beatriu de Pinòs Programme of the Government of Catalonia (2020 BP 00126). Kristen L. Manies acknowledges the support of the US Geological Survey Earth Surface Dynamics Program. Alison K. Paulson and Heather D. Alexander acknowledge Seth Robinson, Eric Borth, Sarah Frankenberg, Aaron Lewis, Brian Izbicki, Clark Thompson, Jill Young, Amanda Ruland, and Elena Forbath for assistance with fieldwork and Valetin Spektor, Nikita Zimov, Sergei Davydov, and Sergei Zimov for contributing extensive knowledge of the region and logistics support. We also acknowledge NSF OPP-2100773. Gerald V. Frost acknowledges funding from the Western Alaska Landscape Conservation Cooperative (WALCC) under award F16AC01215 and the NASA Arctic Boreal Vulnerability Experiment under contract NNH16CP09C. Benjamin V. Gaglioti acknowledges Park Williams for fieldwork, NSF award 2124824, and the Joint Fire Science Program Project 20-2-01-13 for funding. Thanks to Benjamin Maglio and Dana Brown for their assistance in reviewing this paper. Thanks to the Arctic Data Center team for their assistance with archiving the dataset.

Financial support. This research has been supported by the Office of Polar Programs (grant nos. OPP-1708322 and OPP-2116864), the NASA Arctic Boreal Vulnerability Experiment (grant no. 80NSSC22K1244), and the NSF (award no. 2019485).

Review statement. This paper was edited by Jia Yang and reviewed by two anonymous referees.

References

Alexander, H. D., Natali, S. M., Loranty, M. M., Ludwig, S. M., Spektor, V. V., Davydov, S., Zimov, N., Trujillo, I., and Mack, M. C.: Impacts of increased soil burn severity on larch forest regeneration on permafrost soils of far northeastern Siberia, Forest Ecol. Manage., 417, 144–153, https://doi.org/10.1016/j.foreco.2018.03.008, 2018.

Alexander, H. D., Paulson, A. K., DeMarco, J., Hewitt, R., Lichstein, J., Loranty, M. M., Mack, M. C., McEwan, R., Frankenberg, S., and Robinson, S.: Fire influences on forest recovery and associated climate feedbacks in Siberian Larch

Forests, Russia, 2018–2019, Arcit Data Center [data set], https://doi.org/10.18739/A2XG9FB90, 2020.

Amiro, B. D.: Paired-tower measurements of carbon and energy fluxes following disturbance in the boreal forest, Global Change Biol., 7, 253–268, https://doi.org/10.1046/j.1365-2486.2001.00398.x, 2001.

Amiro, B. D., Orchansky, A. L., Barr, A. G., Black, T. A., Chambers, S. D., Chapin Iii, F. S., Goulden, M. L., Litvak, M., Liu, H. P., McCaughey, J. H., McMillan, A., and Randerson, J. T.: The effect of post-fire stand age on the boreal forest energy balance, Agr. Forest Meteorol., 140, 41–50, https://doi.org/10.1016/j.agrformet.2006.02.014, 2006.

Anisimov, O. and Reneva, S.: Permafrost and Changing Climate: The Russian Perspective, Ambio, 35, 169–175, https://doi.org/10.1579/0044-7447(2006)35[169:PACCTR]2.0.CO;2, 2006.

Baillargeon, N., Pold, G., Natali, S. M., and Sistla, S. A.: Lowland tundra plant stoichiometry is somewhat resilient decades following fire despite substantial and sustained shifts in community structure, Arct. Antarct. Alp. Res., 54, 525–536, https://doi.org/10.1080/15230430.2022.2121246, 2022.

Baltzer, J. L., Veness, T., Chasmer, L. E., Sniderhan, A. E., and Quinton, W. L.: Forests on thawing permafrost: fragmentation, edge effects, and net forest loss, Global Change Biol., 20, 824–834, https://doi.org/10.1111/gcb.12349, 2014.

Barichivich, J., Briffa, K. R., Osborn, T. J., Melvin, T. M., and Caesar, J.: Thermal growing season and timing of biospheric carbon uptake across the Northern Hemisphere, Global Biogeochem. Cy., 26, 2012GB004312, https://doi.org/10.1029/2012GB004312, 2012.

Bonnaventure, P. P. and Lamoureux, S. F.: The active layer: A conceptual review of monitoring, modeling techniques and changes in a warming climate, Prog. Phys. Geogr., 37, 352–376, https://doi.org/10.1177/0309133313478314, 2013.

Borge, A. F., Westermann, S., Solheim, I., and Etzelmüller, B.: Strong degradation of palsas and peat plateaus in northern Norway during the last 60 years, The Cryosphere, 11, 1–16, https://doi.org/10.5194/tc-11-1-2017, 2017.

Bret-Harte, M. S., Mack, M. C., Shaver, G. R., Huebner, D. C., Johnston, M., Mojica, C. A., Pizano, C., and Reiskind, J. A.: The response of Arctic vegetation and soils following an unusually severe tundra fire, Philos. T. Roy. Soc. B, 368, 20120490, https://doi.org/10.1098/rstb.2012.0490, 2013.

Brown, D. R. N., Jorgenson, M. T., Douglas, T. A., Romanovsky, V. E., Kielland, K., Hiemstra, C., Euskirchen, E. S., and Ruess, R. W.: Interactive effects of wildfire and climate on permafrost degradation in Alaskan lowland forests, J. Geophys. Res.-Biogeo., 120, 1619–1637, https://doi.org/10.1002/2015JG003033, 2015.

Brown, J., Ferrians, O., Heginbottom, J. A., and Melnikov, E.: Circum-Arctic Map of Permafrost and Ground-Ice Conditions, Version 2, National Snow and Ice Data Center [data set], https://doi.org/10.7265/skbg-kf16, 1998.

Brown, J., Hinkel, K. M., and Nelson, F. E.: The circumpolar active layer monitoring (calm) program: Research designs and initial results, Polar Geogr., 24, 166–258, https://doi.org/10.1080/10889370009377698, 2000.

Buma, B., Hayes, K., Weiss, S., and Lucash, M.: Short-interval fires increasing in the Alaskan boreal forest as fire self-regulation decays across forest types, Sci. Rep., 12, 4901, https://doi.org/10.1038/s41598-022-08912-8, 2022.

Burn, C. R. and Lewkowicz, A. G.: Canadian Landform Examples – 17: Retrogressive thaw slumps, Canadian Geographies/Géographies canadiennes, 34, 273–276, https://doi.org/10.1111/j.1541-0064.1990.tb01092.x, 1990.

Byrne, B., Liu, J., Bowman, K. W., Pascolini-Campbell, M., Chatterjee, A., Pandey, S., Miyazaki, K., Van Der Werf, G. R., Wunch, D., Wennberg, P. O., Roehl, C. M., and Sinha, S.: Carbon emissions from the 2023 Canadian wildfires, Nature, 633, 835–839, https://doi.org/10.1038/s41586-024-07878-z, 2024.

Calvin, K., Dasgupta, D., Krinner, G., Mukherji, A., Thorne, P. W., Trisos, C., Romero, J., Aldunce, P., Barrett, K., Blanco, G., Cheung, W. W. L., Connors, S., Denton, F., Diongue-Niang, A., Dodman, D., Garschagen, M., Geden, O., Hayward, B., Jones, C., Jotzo, F., Krug, T., Lasco, R., Lee, Y.-Y., Masson-Delmotte, V., Meinshausen, M., Mintenbeck, K., Mokssit, A., Otto, F. E. L., Pathak, M., Pirani, A., Poloczanska, E., Pörtner, H.-O., Revi, A., Roberts, D. C., Roy, J., Ruane, A. C., Skea, J., Shukla, P. R., Slade, R., Slangen, A., Sokona, Y., Sörensson, A. A., Tignor, M., Van Vuuren, D., Wei, Y.-M., Winkler, H., Zhai, P., Zommers, Z., Hourcade, J.-C., Johnson, F. X., Pachauri, S., Simpson, N. P., Singh, C., Thomas, A., Totin, E., Arias, P., Bustamante, M., Elgizouli, I., Flato, G., Howden, M., Méndez-Vallejo, C., Pereira, J. J., Pichs-Madruga, R., Rose, S. K., Saheb, Y., Sánchez Rodríguez, R., Ürge-Vorsatz, D., Xiao, C., Yassaa, N., Alegría, A., Armour, K., Bednar-Friedl, B., Blok, K., Cissé, G., Dentener, F., Eriksen, S., Fischer, E., Garner, G., Guivarch, C., Haasnoot, M., Hansen, G., Hauser, M., Hawkins, E., Hermans, T., Kopp, R., Leprince-Ringuet, N., Lewis, J., Ley, D., Ludden, C., Niamir, L., Nicholls, Z., Some, S., Szopa, S., Trewin, B., Van Der Wijst, K.-I., Winter, G., Witting, M., Birt, A., Ha, M., et al.: IPCC, 2023: Climate Change 2023: Synthesis Report, in: Contribution of Working Groups I, II and III to the Sixth Assessment Report of the Intergovernmental Panel on Climate Change, edited by: Core Writing Team, Lee, H., and Romero, J., IPCC – Intergovernmental Panel on Climate Change, Geneva, Switzerland,, https://doi.org/10.59327/IPCC/AR6-9789291691647, 2023.

Chambers, S. D. and Chapin, F. S.: Fire effects on surface-atmosphere energy exchange in Alaskan black spruce ecosystems: Implications for feedbacks to regional climate, J. Geophys. Res., 107, 8145–8162, https://doi.org/10.1029/2001JD000530, 2002.

Chambers, S. D., Beringer, J., Randerson, J. T., and Chapin, F. S.: Fire effects on net radiation and energy partitioning: Contrasting responses of tundra and boreal forest ecosystems, J. Geophys. Res., 110, 2004JD005299, https://doi.org/10.1029/2004JD005299, 2005.

Chebykina, E., Polyakov, V., Abakumov, E., and Petrov, A.: Wildfire Effects on Cryosols in Central Yakutia Region, Russia, Atmosphere, 13, 1889, https://doi.org/10.3390/atmos13111889, 2022.

Clelland, A. A., Marshall, G. J., and Baxter, R.: Evaluating the performance of key ERA-Interim, ERA5 and ERA5-Land climate variables across Siberia, Int. J. Climatol., 44, 2318–2342, https://doi.org/10.1002/joc.8456, 2024.

Dearborn, K. D., Wallace, C. A., Patankar, R., and Baltzer, J. L.: Permafrost thaw in boreal peatlands is rapidly alter-

ing forest community composition, J. Ecol., 109, 1452–1467, https://doi.org/10.1111/1365-2745.13569, 2021.

de Groot, W. J., Flannigan, M. D., and Cantin, A. S.: Climate change impacts on future boreal fire regimes, Forest Ecol. Manage., 294, 35–44, https://doi.org/10.1016/j.foreco.2012.09.027, 2013.

Delcourt, C. J. F., Combee, A., Izbicki, B., Mack, M. C., Maximov, T., Petrov, R., Rogers, B. M., Scholten, R. C., Shestakova, T. A., Van Wees, D., and Veraverbeke, S.: Evaluating the Differenced Normalized Burn Ratio for Assessing Fire Severity Using Sentinel-2 Imagery in Northeast Siberian Larch Forests, Remote Sens., 13, 2311, https://doi.org/10.3390/rs13122311, 2021.

Delcourt, C. J. F., Rogers, B. M., Akhmetzyanov, L., Izbicki, B., Scholten, R. C., Shestakova, T., van Wees, D., Mack, M. C., Sass-Klaassen, U., and Veraverbeke, S.: Burned and Unburned Boreal Larch Forest Site Data, Northeast Siberia, Zenodo [data set], https://doi.org/10.5281/zenodo.10840088, 2024.

Derksen, C., Burgess, D., Duguay, C., Howell, S., Mudryk, L., Smith, S., Thackeray, C., and Kirchmeier-Young, M.: Changes in snow, ice, and permafrost across Canada, in: Canada's Changing Climate Report, Government of Canada, Ottawa, Ontario, 194–260, https://natural-resources.canada.ca/sites/www.nrcan.gc.ca/files/energy/Climate-change/pdf/CCCR-Chapter5-ChangesInSnowIcePermafrostAcrossCanada.pdf (last access: 5 November 2024), 2019.

Descals, A., Gaveau, D. L. A., Verger, A., Sheil, D., Naito, D., and Peñuelas, J.: Unprecedented fire activity above the Arctic Circle linked to rising temperatures, Science, 378, 532–537, https://doi.org/10.1126/science.abn9768, 2022.

Diaz, L. R., Delcourt, C. J. F., Langer, M., Loranty, M. M., Rogers, B. M., Scholten, R. C., Shestakova, T. A., Talucci, A. C., Vonk, J. E., Wangchuk, S., and Veraverbeke, S.: Environmental drivers and remote sensing proxies of post-fire thaw depth in eastern Siberian larch forests, Earth Syst. Dynam., 15, 1459–1482, https://doi.org/10.5194/esd-15-1459-2024, 2024.

Dieleman, C. M., Day, N. J., Holloway, J. E., Baltzer, J., Douglas, T. A., and Turetsky, M. R.: Carbon and nitrogen cycling dynamics following permafrost thaw in the Northwest Territories, Sci. Total Environ., 845, 157288, https://doi.org/10.1016/j.scitotenv.2022.157288, 2022

Dinerstein, E., Olson, D., Joshi, A., Vynne, C., Burgess, N. D., Wikramanayake, E., Hahn, N., Palminteri, S., Hedao, P., Noss, R., Hansen, M., Locke, H., Ellis, E. C., Jones, B., Barber, C. V., Hayes, R., Kormos, C., Martin, V., Crist, E., Sechrest, W., Price, L., Baillie, J. E. M., Weeden, D., Suckling, K., Davis, C., Sizer, N., Moore, R., Thau, D., Birch, T., Potapov, P., Turubanova, S., Tyukavina, A., De Souza, N., Pintea, L., Brito, J. C., Llewellyn, O. A., Miller, A. G., Patzelt, A., Ghazanfar, S. A., Timberlake, J., Klöser, H., Shennan-Farpón, Y., Kindt, R., Lillesø, J.-P. B., Van Breugel, P., Graudal, L., Voge, M., Al-Shammari, K. F., and Saleem, M.: An Ecoregion-Based Approach to Protecting Half the Terrestrial Realm, BioScience, 67, 534–545, https://doi.org/10.1093/biosci/bix014, 2017.

Douglas, T. A., Jorgenson, M. T., Brown, D. R. N., Campbell, S. W., Hiemstra, C. A., Saari, S. P., Bjella, K., and Liljedahl, A. K.: Degrading permafrost mapped with electrical resistivity tomography, airborne imagery and LiDAR, and seasonal thaw measurements, Geophysics, 81, WA71–WA85, https://doi.org/10.1190/geo2015-0149.1, 2016.

Fedorov, A. N.: Permafrost Landscape Research in the Northeast of Eurasia, Earth, 3, 460–478, https://doi.org/10.3390/earth3010028, 2022.

Fisher, J. P., Estop-Aragonés, C., Thierry, A., Charman, D. J., Wolfe, S. A., Hartley, I. P., Murton, J. B., Williams, M., and Phoenix, G. K.: The influence of vegetation and soil characteristics on active-layer thickness of permafrost soils in boreal forest, Global Change Biol., 22, 3127–3140, https://doi.org/10.1111/gcb.13248, 2016.

Fraser, R., Kokelj, S., Lantz, T., McFarlane-Winchester, M., Olthof, I., and Lacelle, D.: Climate Sensitivity of High Arctic Permafrost Terrain Demonstrated by Widespread Ice-Wedge Thermokarst on Banks Island, Remote Sens., 10, 954, https://doi.org/10.3390/rs10060954, 2018.

Freitag, D. and McFadden, T.: Introduction to Cold Regions Engineering, ASCE Press, 166–169, 1997.

Frost, G. V., Loehman, R. A., Nelson, P. R., and Paradis, D. P.: ABoVE: Vegetation Composition across Fire History Gradients on the Y-K Delta, Alaska, ORNL DAAC [data set], https://doi.org/10.3334/ORNLDAAC/1772, 2020.

Gaglioti, B. V., Berner, L. T., Jones, B. M., Orndahl, K. M., Williams, A. P., Andreu-Hayles, L., D'Arrigo, R. D., Goetz, S. J., and Mann, D. H.: Tussocks Enduring or Shrubs Greening: Alternate Responses to Changing Fire Regimes in the Noatak River Valley, Alaska, J. Geophys. Res.-Biogeo., 126, 1–21, https://doi.org/10.1029/2020JG006009, 2021.

Gasser, T., Kechiar, M., Ciais, P., Burke, E. J., Kleinen, T., Zhu, D., Huang, Y., Ekici, A., and Obersteiner, M.: Path-dependent reductions in CO_2 emission budgets caused by permafrost carbon release, Nat. Geosci., 11, 830–835, https://doi.org/10.1038/s41561-018-0227-0, 2018.

Gibson, C. M., Chasmer, L. E., Thompson, D. K., Quinton, W. L., Flannigan, M. D., and Olefeldt, D.: Wildfire as a major driver of recent permafrost thaw in boreal peatlands, Nat. Commun., 9, 3041, https://doi.org/10.1038/s41467-018-05457-1, 2018.

Gibson, C. M., Brinkman, T., Cold, H., Brown, D., and Turetsky, M.: Identifying increasing risks of hazards for northern land-users caused by permafrost thaw: integrating scientific and community-based research approaches, Environ. Res. Lett., 16, 064047, https://doi.org/10.1088/1748-9326/abfc79, 2021.

Gorelick, N., Hancher, M., Dixon, M., Ilyushchenko, S., Thau, D., and Moore, R.: Google Earth Engine: Planetary-scale geospatial analysis for everyone, Remote Sens. Environ., 202, 18–27, https://doi.org/10.1016/j.rse.2017.06.031, 2017.

Grünberg, I., Groenke, B., Westermann, S., and Boike, J.: Permafrost and Active Layer Temperature and Freeze/Thaw Timing Reflect Climatic Trends at Bayelva, Svalbard, J. Geophys. Res.-Earth, 129, e2024JF007648, https://doi.org/10.1029/2024JF007648, 2024.

Hanes, C. C., Wang, X., Jain, P., Parisien, M.-A., Little, J. M., and Flannigan, M. D.: Fire-regime changes in Canada over the last half century, Can. J. Forest Res., 49, 256–269, https://doi.org/10.1139/cjfr-2018-0293, 2019.

Harden, J. W., Manies, K. L., Turetsky, M. R., and Neff, J. C.: Effects of wildfire and permafrost on soil organic matter and soil climate in interior Alaska: effects of wildfire and permafrost on soil, Global Change Biol., 12, 2391–2403, https://doi.org/10.1111/j.1365-2486.2006.01255.x, 2006.

Harris, S. A., Permafrost Subcommittee, Associate Committee on Geotechnical Research, and National Research Council of Canada (Eds.): Glossary of permafrost and related ground-ice terms, Ottawa, Ontario, Canada, 156 pp., https://doi.org/10.4224/20386561, 1988.

Hayes, K. and Buma, B.: Effects of short-interval disturbances continue to accumulate, overwhelming variability in local resilience, Ecosphere, 12, e03379, https://doi.org/10.1002/ecs2.3379, 2021.

Heim, R. J., Bucharova, A., Brodt, L., Kamp, J., Rieker, D., Soromotin, A. V., Yurtaev, A., and Hölzel, N.: Post-fire vegetation succession in the Siberian subarctic tundra over 45 years, Sci. Total Environ., 760, 143425, https://doi.org/10.1016/j.scitotenv.2020.143425, 2021.

Helbig, M., Daw, L., Iwata, H., Rudaitis, L., Ueyama, M., and Živković, T.: Boreal Forest Fire Causes Daytime Surface Warming During Summer to Exceed Surface Cooling During Winter in North America, AGU Adv., 5, e2024AV001327, https://doi.org/10.1029/2024AV001327, 2024.

Hollingsworth, T. N., Breen, A., Mack, M. C., and Hewitt, R. E.: Seward Peninsula post-fire vegetation and soil data from multiple burns occurring from 1971 to 2012: "SPANFire" Study Sites, http://www.lter.uaf.edu/data/data-detail/id/752 (last access: 15 February 2025), 2020.

Hollingsworth, T. N., Breen, A. L., Hewitt, R. E., and Mack, M. C.: Does fire always accelerate shrub expansion in Arctic tundra? Examining a novel grass-dominated successional trajectory on the Seward Peninsula, Arct. Antarct. Alp. Res., 53, 93–109, https://doi.org/10.1080/15230430.2021.1899562, 2021.

Holloway, J.: Impacts of forest fire on permafrost in the discontinuous zones of northwestern Canada, University of Ottawa, Ottawa, Ontario, https://doi.org/10.20381/ruor-25410, 2020.

Holloway, J. E. and Lewkowicz, A. G.: Half a century of discontinuous permafrost persistence and degradation in western Canada, Permafrost Periglac. Process., 31, 85–96, https://doi.org/10.1002/ppp.2017, 2020.

Holloway, J. E., Lewkowicz, A. G., Douglas, T. A., Li, X., Turetsky, M. R., Baltzer, J. L., and Jin, H.: Impact of wildfire on permafrost landscapes: A review of recent advances and future prospects, Permafrost Periglac. Process., 31, 371–382, https://doi.org/10.1002/ppp.2048, 2020.

Holloway, J. E., Lewkowicz, T., Baltzer, J. L., Turetsky, M. R., and Wolfe, S. A.: Frost table depths from 1–5 years post-fire in the boreal forest, Northwest Territories, Canada [computer file], 2024.

Hu, G., Zhao, L., Li, R., Wu, X., Wu, T., Zou, D., Zhu, X., Jie, C., Su, Y., Hao, J., and Li, W.: Dynamics of the freeze–thaw front of active layer on the Qinghai-Tibet Plateau, Geoderma, 430, 116353, https://doi.org/10.1016/j.geoderma.2023.116353, 2023.

Huang, B., Lu, F., Wang, X., Zheng, H., Wu, X., Zhang, L., Yuan, Y., and Ouyang, Z.: Ecological restoration is crucial in mitigating carbon loss caused by permafrost thawing on the Qinghai-Tibet Plateau, Commun. Earth Environ., 5, 341, https://doi.org/10.1038/s43247-024-01511-7, 2024.

Hugelius, G., Strauss, J., Zubrzycki, S., Harden, J. W., Schuur, E. A. G., Ping, C.-L., Schirrmeister, L., Grosse, G., Michaelson, G. J., Koven, C. D., O'Donnell, J. A., Elberling, B., Mishra, U., Camill, P., Yu, Z., Palmtag, J., and Kuhry, P.: Estimated stocks of circumpolar permafrost carbon with quantified uncertainty ranges and identified data gaps, Biogeosciences, 11, 6573–6593, https://doi.org/10.5194/bg-11-6573-2014, 2014.

Jafarov, E. E., Romanovsky, V. E., Genet, H., McGuire, A. D., and Marchenko, S. S.: The effects of fire on the thermal stability of permafrost in lowland and upland black spruce forests of interior Alaska in a changing climate, Environ. Res. Lett., 8, 035030, https://doi.org/10.1088/1748-9326/8/3/035030, 2013.

Jiang, Y., Rocha, A. V., O'Donnell, J. A., Drysdale, J. A., Rastetter, E. B., Shaver, G. R., and Zhuang, Q.: Contrasting soil thermal responses to fire in Alaskan tundra and boreal forest: Contrasting soil thermal responses, J. Geophys. Res.-Earth, 120, 363–378, https://doi.org/10.1002/2014JF003180, 2015.

Jones, B. M., Grosse, G., Arp, C. D., Miller, E., Liu, L., Hayes, D. J., and Larsen, C. F.: Recent Arctic tundra fire initiates widespread thermokarst development, Sci. Rep,. 5, 15865, https://doi.org/10.1038/srep15865, 2015.

Jones, B. M., Kanevskiy, M. Z., Shur, Y., Gaglioti, B. V., Jorgenson, M. T., Ward Jones, M. K., Veremeeva, A., Miller, E. A., and Jandt, R.: Post-fire stabilization of thaw-affected permafrost terrain in northern Alaska, Sci. Rep., 14, 8499, https://doi.org/10.1038/s41598-024-58998-5, 2024.

Kasischke, E. S., Verbyla, D. L., Rupp, T. S., McGuire, A. D., Murphy, K. A., Jandt, R., Barnes, J. L., Hoy, E. E., Duffy, P. A., Calef, M., and Turetsky, M. R.: Alaska's changing fire regime — implications for the vulnerability of its boreal forests, Can. J. Forest Res., 40, 1313–1324, https://doi.org/10.1139/X10-098, 2010.

Kirdyanov, A. V., Saurer, M., Siegwolf, R., Knorre, A. A., Prokushkin, A. S., Churakova (Sidorova), O. V., Fonti, M. V., and Büntgen, U.: Long-term ecological consequences of forest fires in the continuous permafrost zone of Siberia, Environ. Res. Lett., 15, 034061, https://doi.org/10.1088/1748-9326/ab7469, 2020.

Knoblauch, C., Beer, C., Liebner, S., Grigoriev, M. N., and Pfeiffer, E.-M.: Methane production as key to the greenhouse gas budget of thawing permafrost, Nat. Clim. Change, 8, 309–312, https://doi.org/10.1038/s41558-018-0095-z, 2018.

Kurylyk, B. L. and Hayashi, M.: Improved Stefan Equation Correction Factors to Accommodate Sensible Heat Storage during Soil Freezing or Thawing, Permafrost Periglac., 27, 189–203, https://doi.org/10.1002/ppp.1865, 2016.

Lewkowicz, A. G.: Dynamics of active-layer detachment failures, Fosheim Peninsula, Ellesmere Island, Nunavut, Canada, Permafrost Periglac., 18, 89–103, https://doi.org/10.1002/ppp.578, 2007.

Li, X., Jin, H., He, R., Huang, Y., Wang, H., Luo, D., Jin, X., Lü, L., Wang, L., Li, W., Wei, C., Chang, X., Yang, S., and Yu, S.: Effects of forest fires on the permafrost environment in the northern Da Xing'anling (Hinggan) mountains, Northeast China, Permafrost Periglac., 30, 163–177, https://doi.org/10.1002/ppp.2001, 2019.

Liljedahl, A. K., Boike, J., Daanen, R. P., Fedorov, A. N., Frost, G. V., Grosse, G., Hinzman, L. D., Iijma, Y., Jorgenson, J. C., Matveyeva, N., Necsoiu, M., Raynolds, M. K., Romanovsky, V. E., Schulla, J., Tape, K. D., Walker, D. A., Wilson, C. J., Yabuki, H., and Zona, D.: Pan-Arctic ice-wedge degradation in warming permafrost and its influence on tundra hydrology, Nat. Geosci., 9, 312–318, https://doi.org/10.1038/ngeo2674, 2016.

Liu, H., Randerson, J. T., Lindfors, J., and Chapin, F. S.: Changes in the surface energy budget after fire in boreal ecosystems of

interior Alaska: An annual perspective, J. Geophys. Res., 110, 2004JD005158, https://doi.org/10.1029/2004JD005158, 2005.

Liu, L., Zhuang, Q., Zhao, D., Wei, J., and Zheng, D.: The Fate of Deep Permafrost Carbon in Northern High Latitudes in the 21st Century: A Process-Based Modeling Analysis, Earth's Future, 12, e2024EF004996, https://doi.org/10.1029/2024EF004996, 2024.

López-Blanco, E., Topp-Jørgensen, E., Christensen, T. R., Rasch, M., Skov, H., Arndal, M. F., Bret-Harte, M. S., Callaghan, T. V., and Schmidt, N. M.: Towards an increasingly biased view on Arctic change, Nat. Clim. Change, 14, 152–155, https://doi.org/10.1038/s41558-023-01903-1, 2024.

Loranty, M. M., Natali, S. M., Berner, L. T., Goetz, S. J., Holmes, R. M., Davydov, S. P., Zimov, N. S., and Zimov, S. A.: Siberian tundra ecosystem vegetation and carbon stocks four decades after wildfire, J. Geophys. Res.-Biogeo., 119, 2144–2154, https://doi.org/10.1002/2014JG002730, 2014.

Loranty, M. M., Lieberman-Cribbin, W., Berner, L. T., Natali, S. M., Goetz, S. J., Alexander, H. D., and Kholodov, A. L.: Spatial variation in vegetation productivity trends, fire disturbance, and soil carbon across arctic-boreal permafrost ecosystems, Environ. Res. Lett., 11, 095008, https://doi.org/10.1088/1748-9326/11/9/095008, 2016.

Lytkina, L.: Post-fire dynamics of forest growth conditions in larch forests of Central Yakutia, Geogr. Nat. Resour., 2, 181–185, 2008.

Mamet, S. D., Chun, K. P., Kershaw, G. G. L., Loranty, M. M., and Peter Kershaw, G.: Recent Increases in Permafrost Thaw Rates and Areal Loss of Palsas in the Western Northwest Territories, Canada, Permafrost Periglac., 28, 619–633, https://doi.org/10.1002/ppp.1951, 2017.

Manies, K. L., Harden, J. W., Silva, S. R., Briggs, P. H., and Schmid, B. M.: Soil Data from Picea mariana Stands near Delta Junction, Alaska of Different Ages and Soil Drainage Type, US Geological Survey, https://pubs.usgs.gov/of/2004/1271/ (last access: 15 February 2025), 2004.

McCarty, J. L., Aalto, J., Paunu, V.-V., Arnold, S. R., Eckhardt, S., Klimont, Z., Fain, J. J., Evangeliou, N., Venäläinen, A., Tchebakova, N. M., Parfenova, E. I., Kupiainen, K., Soja, A. J., Huang, L., and Wilson, S.: Reviews and syntheses: Arctic fire regimes and emissions in the 21st century, Biogeosciences, 18, 5053–5083, https://doi.org/10.5194/bg-18-5053-2021, 2021.

Moskalenko, N. G.: Anthropogenic Dynamics of Vegetation in the Plains of the Russian Permafrost, Nauka, Novosibirsk, Russia, p. 280, 1999.

Muñoz Sabater, J.: ERA5-Land Daily Aggregated-ECMWF Climate Reanalysis, Copernicus Climate Change Service (C3S) Climate Data Store (CDS) [data set], https://doi.org/10.24381/cds.68d2bb30, 2019.

Muñoz-Sabater, J., Dutra, E., Agustí-Panareda, A., Albergel, C., Arduini, G., Balsamo, G., Boussetta, S., Choulga, M., Harrigan, S., Hersbach, H., Martens, B., Miralles, D. G., Piles, M., Rodríguez-Fernández, N. J., Zsoter, E., Buontempo, C., and Thépaut, J.-N.: ERA5-Land: a state-of-the-art global reanalysis dataset for land applications, Earth Syst. Sci. Data, 13, 4349–4383, https://doi.org/10.5194/essd-13-4349-2021, 2021.

Natali, S.: Yukon-Kuskokwim Delta fire: thaw depth, soil temperature, and point-intercept vegetation, Yukon-Kuskokwim Delta Alaska, 2015–2019, Arctic Data Center [data set], https://doi.org/10.18739/A2707WP16, 2018.

Natali, S., Kholodov, A. L., and Loranty, M. M.: Thaw depth and organic layer depth from Alaska borehole sites, 2015, 2017, 2018 (ViPER Project), Arctic Data Center [data set], https://doi.org/10.18739/A22J6848J, 2016.

Natali, S., Ludwig, S., Minions, C., and Watts, J. D.: ABoVE: Thaw Depth at Selected Unburned and Burned Sites Across Alaska, 2016–2017, ORNL DAAC [data set], https://doi.org/10.3334/ORNLDAAC/1579, 2018.

Natali, S. M., Holdren, J. P., Rogers, B. M., Treharne, R., Duffy, P. B., Pomerance, R., and MacDonald, E.: Permafrost carbon feedbacks threaten global climate goals, P. Natl. Acad. Sci. USA, 118, e2100163118, https://doi.org/10.1073/pnas.2100163118, 2021.

Nelson, F. E., Shiklomanov, N. I., and Nyland, K. E.: Cool, CALM, collected: the Circumpolar Active Layer Monitoring program and network, Polar Geogr., 44, 155–166, https://doi.org/10.1080/1088937X.2021.1988001, 2021.

Nossov, D. R., Torre Jorgenson, M., Kielland, K., and Kanevskiy, M. Z.: Edaphic and microclimatic controls over permafrost response to fire in interior Alaska, Environ. Res. Lett., 8, 035013, https://doi.org/10.1088/1748-9326/8/3/035013, 2013.

O'Donnell, J. A., Turetsky, M. R., Harden, J. W., Manies, K. L., Pruett, L. E., Shetler, G., and Neff, J. C.: Interactive Effects of Fire, Soil Climate, and Moss on CO_2 Fluxes in Black Spruce Ecosystems of Interior Alaska, Ecosystems, 12, 57–72, https://doi.org/10.1007/s10021-008-9206-4, 2009.

O'Donnell, J. A., Harden, J. W., and Manies, K. L.: Soil physical, chemical, and gas flux characterization from Picea mariana stands near Erickson Creek, Alaska, US Geological Survey, https://pubs.usgs.gov/of/2011/1153/ (last access: 15 February 2025), 2011a.

O'Donnell, J. A., Harden, J. W., McGUIRE, A. D., Kanevskiy, M. Z., Jorgenson, M. T., and Xu, X.: The effect of fire and permafrost interactions on soil carbon accumulation in an upland black spruce ecosystem of interior Alaska, Global Change Biol., 17, 1461–1474, https://doi.org/10.1111/j.1365-2486.2010.02358.x, 2011b.

O'Donnell, J. A., Harden, J. W., McGuire, A. D., and Romanovsky, V. E.: Exploring the sensitivity of soil carbon dynamics to climate change, fire disturbance and permafrost thaw in a black spruce ecosystem, Biogeosciences, 8, 1367–1382, https://doi.org/10.5194/bg-8-1367-2011, 2011c.

O'Donnell, J. A., Harden, J. W., Manies, K. L., Jorgenson, M. T., and Kanevskiy, M. Z.: Soil data from fire and permafrost-thaw chronosequences in upland Picea mariana stands near Hess Creek and Tok, Alaska, US Geological Survey, https://doi.org/10.3133/ofr20131045, 2013.

O'Neill, H. B., Smith, S. L., Burn, C. R., Duchesne, C., and Zhang, Y.: Widespread Permafrost Degradation and Thaw Subsidence in Northwest Canada, J. Geophys. Res.-Earth, 128, e2023JF007262, https://doi.org/10.1029/2023JF007262, 2023.

Osterkamp, T. E.: Freezing and thawing of soils and permafrost containing unfrozen water or brine, Water Resour. Res., 23, 2279–2285, https://doi.org/10.1029/WR023i012p02279, 1987.

Osterkamp, T. E. and Burn, C. R.: Permafrost, in: Encyclopedia of Atmospheric Sciences, Academic Press, ISBN 9780122270901, 2002.

Painter, S. L., Coon, E. T., Khattak, A. J., and Jastrow, J. D.: Drying of tundra landscapes will limit subsidence-induced acceleration of permafrost thaw, P. Natl. Acad. Sci. USA, 120, e2212171120, https://doi.org/10.1073/pnas.2212171120, 2023.

Peng, X., Zhang, T., Frauenfeld, O. W., Mu, C., Wang, K., Wu, X., Guo, D., Luo, J., Hjort, J., Aalto, J., Karjalainen, O., and Luoto, M.: Active Layer Thickness and Permafrost Area Projections for the 21st Century, Earth's Future, 11, e2023EF003573, https://doi.org/10.1029/2023EF003573, 2023.

Petrov, M. I., Fedorov, A. N., Konstantinov, P. Y., and Argunov, R. N.: Variability of Permafrost and Landscape Conditions Following Forest Fires in the Central Yakutian Taiga Zone, Land, 11, 496, https://doi.org/10.3390/land11040496, 2022.

Phillips, C. A., Rogers, B. M., Elder, M., Cooperdock, S., Moubarak, M., Randerson, J. T., and Frumhoff, P. C.: Escalating carbon emissions from North American boreal forest wildfires and the climate mitigation potential of fire management, Sci. Adv., 8, eabl7161, https://doi.org/10.1126/sciadv.abl7161, 2022.

Rantanen, M., Kämäräinen, M., Niittynen, P., Phoenix, G. K., Lenoir, J., Maclean, I., Luoto, M., and Aalto, J.: Bioclimatic atlas of the terrestrial Arctic, Sci. Data, 10, 40, https://doi.org/10.1038/s41597-023-01959-w, 2023.

Riseborough, D., Shiklomanov, N., Etzelmüller, B., Gruber, S., and Marchenko, S.: Recent advances in permafrost modelling, Permafrost Periglac. Proc., 19, 137–156, https://doi.org/10.1002/ppp.615, 2008.

Rocha, A. V. and Shaver, G. R.: Postfire energy exchange in arctic tundra: the importance and climatic implications of burn severity, Global Change Biol., 17, 2831–2841, https://doi.org/10.1111/j.1365-2486.2011.02441.x, 2011.

Rocha, A. V., Loranty, M. M., Higuera, P. E., Mack, M. C., Hu, F. S., Jones, B. M., Breen, A. L., Rastetter, E. B., Goetz, S. J., and Shaver, G. R.: The footprint of Alaskan tundra fires during the past half-century: implications for surface properties and radiative forcing, Environ. Res. Lett., 7, 044039, https://doi.org/10.1088/1748-9326/7/4/044039, 2012.

Romanovsky, V. E. and Osterkamp, T. E.: Effects of unfrozen water on heat and mass transport processes in the active layer and permafrost, Permafrost Periglac. Process., 11, 219–239, https://doi.org/10.1002/1099-1530(200007/09)11:3<219::AID-PPP352>3.0.CO;2-7, 2000.

Romanovsky, V. E., Smith, S. L., and Christiansen, H. H.: Permafrost thermal state in the polar Northern Hemisphere during the international polar year 2007–2009: a synthesis, Permafrost Periglac., 21, 106–116, https://doi.org/10.1002/ppp.689, 2010.

Rouse, W. R.: Microclimatic Changes Accompanying Burning in Subarctic Lichen Woodland, Arct. Alp. Res., 8, 357–376, https://doi.org/10.2307/1550439, 1976.

Rudy, A. C. A., Lamoureux, S. F., Treitz, P., Ewijk, K. V., Bonnaventure, P. P., and Budkewitsch, P.: Terrain Controls and Landscape-Scale Susceptibility Modelling of Active-Layer Detachments, Sabine Peninsula, Melville Island, Nunavut: Landscape-Scale Modelling of Active-Layer Detachment Susceptibility, Permafrost Periglac. Process., 28, 79–91, https://doi.org/10.1002/ppp.1900, 2017.

Sannel, A. B. K. and Kuhry, P.: Warming-induced destabilization of peat plateau/thermokarst lake complexes, J. Geophys. Res., 116, G03035, https://doi.org/10.1029/2010JG001635, 2011.

Schädel, C., Rogers, B. M., Lawrence, D. M., Koven, C. D., Brovkin, V., Burke, E. J., Genet, H., Huntzinger, D. N., Jafarov, E., McGuire, A. D., Riley, W. J., and Natali, S. M.: Earth system models must include permafrost carbon processes, Nat. Clim. Chang., 14, 114–116, https://doi.org/10.1038/s41558-023-01909-9, 2024.

Schaefer, K., Lantuit, H., Romanovsky, V. E., Schuur, E. A. G., and Witt, R.: The impact of the permafrost carbon feedback on global climate, Environ. Res. Lett., 9, 085003, https://doi.org/10.1088/1748-9326/9/8/085003, 2014.

Scheer, J., Caduff, R., How, P., Marcer, M., Strozzi, T., Bartsch, A., and Ingeman-Nielsen, T.: Thaw-Season InSAR Surface Displacements and Frost Susceptibility Mapping to Support Community-Scale Planning in Ilulissat, West Greenland, Remote Sens., 15, 3310, https://doi.org/10.3390/rs15133310, 2023.

Scholten, R. C., Coumou, D., Luo, F., and Veraverbeke, S.: Early snowmelt and polar jet dynamics co-influence recent extreme Siberian fire seasons, Science, 378, 1005–1009, https://doi.org/10.1126/science.abn4419, 2022.

Schuur, E. A. G., McGuire, A. D., Schädel, C., Grosse, G., Harden, J. W., Hayes, D. J., Hugelius, G., Koven, C. D., Kuhry, P., Lawrence, D. M., Natali, S. M., Olefeldt, D., Romanovsky, V. E., Schaefer, K., Turetsky, M. R., Treat, C. C., and Vonk, J. E.: Climate change and the permafrost carbon feedback, Nature, 520, 171–179, https://doi.org/10.1038/nature14338, 2015.

Schuur, E. A. G., Abbott, B. W., Commane, R., Ernakovich, J., Euskirchen, E., Hugelius, G., Grosse, G., Jones, M., Koven, C., Leshyk, V., Lawrence, D., Loranty, M. M., Mauritz, M., Olefeldt, D., Natali, S., Rodenhizer, H., Salmon, V., Schädel, C., Strauss, J., Treat, C., and Turetsky, M.: Permafrost and Climate Change: Carbon Cycle Feedbacks From the Warming Arctic, Annu. Rev. Environ. Resour., 47, 343–371, https://doi.org/10.1146/annurev-environ-012220-011847, 2022.

See, C. R., Virkkala, A.-M., Natali, S. M., Rogers, B. M., Mauritz, M., Biasi, C., Bokhorst, S., Boike, J., Bret-Harte, M. S., Celis, G., Chae, N., Christensen, T. R., Murner, S. J., Dengel, S., Dolman, H., Edgar, C. W., Elberling, B., Emmerton, C. A., Euskirchen, E. S., Göckede, M., Grelle, A., Heffernan, L., Helbig, M., Holl, D., Humphreys, E., Iwata, H., Järveoja, J., Kobayashi, H., Kochendorfer, J., Kolari, P., Kotani, A., Kutzbach, L., Kwon, M. J., Lathrop, E. R., López-Blanco, E., Mammarella, I., Marushchak, M. E., Mastepanov, M., Matsuura, Y., Merbold, L., Meyer, G., Minions, C., Nilsson, M. B., Nojeim, J., Oberbauer, S. F., Olefeldt, D., Park, S.-J., Parmentier, F.-J. W., Peichl, M., Peter, D., Petrov, R., Poyatos, R., Prokushkin, A. S., Quinton, W., Rodenhizer, H., Sachs, T., Savage, K., Schulze, C., Sjögersten, S., Sonnentag, O., St. Louis, V. L., Torn, M. S., Tuittila, E.-S., Ueyama, M., Varlagin, A., Voigt, C., Watts, J. D., Zona, D., Zyryanov, V. I., and Schuur, E. A. G.: Decadal increases in carbon uptake offset by respiratory losses across northern permafrost ecosystems, Nat. Clim. Change, 14, 853–862, https://doi.org/10.1038/s41558-024-02057-4, 2024.

Shiklomanov, N. I., Streletskiy, D. A., Nelson, F. E., Hollister, R. D., Romanovsky, V. E., Tweedie, C. E., Bockheim, J. G., and Brown, J.: Decadal variations of active-layer thickness in moisture-controlled landscapes, Barrow, Alaska, J. Geophys. Res., 115, G00I04, https://doi.org/10.1029/2009JG001248, 2010.

Shur, Y., Hinkel, K. M., and Nelson, F. E.: The transient layer: implications for geocryology and climate-change science, Per-

mafrost Periglac., 16, 5–17, https://doi.org/10.1002/ppp.518, 2005.

Sizov, O., Soromotin, A., and Brodt, L.: Temperature of the active layer in the forest-tundra zone in the north of Western Siberia (Pangody) forest-tundra zone in the north of Western Siberia, Zenodo [data set], https://doi.org/10.5281/zenodo.4285650, 2020.

Smith, S. L. and Burgess, M.: Sensitivity of permafrost to climate warming in Canada, Natural Resources Canada, https://doi.org/10.4095/216137, 2004.

Smith, S. L., Romanovsky, V. E., Lewkowicz, A. G., Burn, C. R., Allard, M., Clow, G. D., Yoshikawa, K., and Throop, J.: Thermal state of permafrost in North America: a contribution to the international polar year, Permafrost Periglac., 21, 117–135, https://doi.org/10.1002/ppp.690, 2010.

Smith, S. L., Riseborough, D. W., and Bonnaventure, P. P.: Eighteen Year Record of Forest Fire Effects on Ground Thermal Regimes and Permafrost in the Central Mackenzie Valley, NWT, Canada, Permafrost Periglac., 26, 289–303, https://doi.org/10.1002/ppp.1849, 2015.

Strand, S. M., Christiansen, H. H., Johansson, M., Åkerman, J., and Humlum, O.: Active layer thickening and controls on interannual variability in the Nordic Arctic compared to the circum-Arctic, Permafrost Periglac., 32, 47–58, https://doi.org/10.1002/ppp.2088, 2021.

Strauss, J., Laboor, S., Schirrmeister, L., Fedorov, A. N., Fortier, D., Froese, D., Fuchs, M., Günther, F., Grigoriev, M., Harden, J., Hugelius, G., Jongejans, L. L., Kanevskiy, M., Kholodov, A., Kunitsky, V., Kraev, G., Lozhkin, A., Rivkina, E., Shur, Y., Siegert, C., Spektor, V., Streletskaya, I., Ulrich, M., Vartanyan, S., Veremeeva, A., Anthony, K. W., Wetterich, S., Zimov, N., and Grosse, G.: Circum-Arctic Map of the Yedoma Permafrost Domain, Front. Earth Sci., 9, 758360, https://doi.org/10.3389/feart.2021.758360, 2021.

Streletskiy, D. A., Suter, L. J., Shiklomanov, N. I., Porfiriev, B. N., and Eliseev, D. O.: Assessment of climate change impacts on buildings, structures and infrastructure in the Russian regions on permafrost, Environ. Res. Lett., 14, 025003, https://doi.org/10.1088/1748-9326/aaf5e6, 2019.

Talucci, A., Loranty, M., Holloway, J., Rogers, B., Alexander, H., Baillargeon, N., Baltzer, J., Berner, L., Breen, A., Brodt, L., Buma, B., Delcourt, C., Diaz, L., Dieleman, C., Douglas, T., Frost, G., Gaglioti, B., Hewitt, R., Hollingsworth, T., Jorgenson, M. T., Lara, M., Loehman, R., Mack, M., Manies, K., Minions, C., Natali, S., O'Donnell, J., Olefeldt, D., Paulson, A., Rocha, A., Saperstein, L., Shestakova, T., Sistla, S., Oleg, S., Soromotin, A., Turetsky, M., Veraverbeke, S., and Walvoord, M.: FireALT dataset: estimated active layer thickness for paired burned unburned sites measured from 2001–2023, Arctic Data Center [code and data set], https://doi.org/10.18739/A2RN3092P, 2024.

Toevs, G. R., Karl, J. W., Taylor, J. J., Spurrier, C. S., Karl, M. "S"., Bobo, M. R., and Herrick, J. E.: Consistent Indicators and Methods and a Scalable Sample Design to Meet Assessment, Inventory, and Monitoring Information Needs Across Scales, Rangelands, 33, 14–20, https://doi.org/10.2111/1551-501X-33.4.14, 2011.

Treharne, R., Rogers, B. M., Gasser, T., MacDonald, E., and Natali, S.: Identifying Barriers to Estimating Carbon Release From Interacting Feedbacks in a Warming Arctic, Front. Clim., 3, 716464, https://doi.org/10.3389/fclim.2021.716464, 2022.

Turetsky, M. R., Abbott, B. W., Jones, M. C., Anthony, K. W., Olefeldt, D., Schuur, E. A. G., Grosse, G., Kuhry, P., Hugelius, G., Koven, C., Lawrence, D. M., Gibson, C., Sannel, A. B. K., and McGuire, A. D.: Carbon release through abrupt permafrost thaw, Nat. Geosci., 13, 138–143, https://doi.org/10.1038/s41561-019-0526-0, 2020.

Wang, Z., Schaaf, C. B., Chopping, M. J., Strahler, A. H., Wang, J., Román, M. O., Rocha, A. V., Woodcock, C. E., and Shuai, Y.: Evaluation of Moderate-resolution Imaging Spectroradiometer (MODIS) snow albedo product (MCD43A) over tundra, Remote Sens. Environ., 117, 264–280, https://doi.org/10.1016/j.rse.2011.10.002, 2012.

Wickham, H., Averick, M., Bryan, J., Chang, W., McGowan, L., François, R., Grolemund, G., Hayes, A., Henry, L., Hester, J., Kuhn, M., Pedersen, T., Miller, E., Bache, S., Müller, K., Ooms, J., Robinson, D., Seidel, D., Spinu, V., Takahashi, K., Vaughan, D., Wilke, C., Woo, K., and Yutani, H.: Welcome to the Tidyverse, J. Open Sour. Softw., 4, 1686, https://doi.org/10.21105/joss.01686, 2019.

Wotton, B. M., Flannigan, M. D., and Marshall, G. A.: Potential climate change impacts on fire intensity and key wildfire suppression thresholds in Canada, Environ. Res. Lett., 12, 095003, https://doi.org/10.1088/1748-9326/aa7e6e, 2017.

Yokohata, T., Saito, K., Ito, A., Ohno, H., Tanaka, K., Hajima, T., and Iwahana, G.: Future projection of greenhouse gas emissions due to permafrost degradation using a simple numerical scheme with a global land surface model, Prog. Earth Planet. Sci., 7, 56, https://doi.org/10.1186/s40645-020-00366-8, 2020.

York, A., Bhatt, U. S., Gargulinski, E., Grabinski, Z., Jain, P., Soja, A., Thoman, R. L., Ziel, R., Alaska Center for Climate Assessment and Policy (US), International Arctic Research Center, United States, National Oceanic and Atmospheric Administration. Office of Oceanic and Atmospheric Research, and Cooperative Institute for Research in the Atmosphere (Fort Collins, Colo.): Arctic Report Card 2020: Wildland Fire in High Northern Latitudes, NOAA, https://doi.org/10.25923/2GEF-3964, 2020.

Zhang, Y., Chen, W., and Riseborough, D. W.: Transient projections of permafrost distribution in Canada during the 21st century under scenarios of climate change, Global Planet. Change, 60, 443–456, https://doi.org/10.1016/j.gloplacha.2007.05.003, 2008.

Zhang, Y., Wolfe, S. A., Morse, P. D., Olthof, I., and Fraser, R. H.: Spatiotemporal impacts of wildfire and climate warming on permafrost across a subarctic region, Canada, J. Geophys. Res.-Earth, 120, 2338–2356, https://doi.org/10.1002/2015JF003679, 2015.

Zheng, B., Ciais, P., Chevallier, F., Yang, H., Canadell, J. G., Chen, Y., Van Der Velde, I. R., Aben, I., Chuvieco, E., Davis, S. J., Deeter, M., Hong, C., Kong, Y., Li, H., Li, H., Lin, X., He, K., and Zhang, Q.: Record-high CO_2 emissions from boreal fires in 2021, Science, 379, 912–917, https://doi.org/10.1126/science.ade0805, 2023.